The Astrophysical Journal, 801:143 (28pp), 2015 March 10 doi:10.1088/0004-637X/801/2/143

DOES THE PRESENCE OF PLANETS AFFECT THE FREQUENCY AND PROPERTIES OF EXTRASOLAR KUIPER BELTS? RESULTS FROM THE *HERSCHEL* DEBRIS AND DUNES SURVEYS

A. Moro-Martín[1,2], J. P. Marshall[3,4,5], G. Kennedy[6], B. Sibthorpe[7], B. C. Matthews[8,9], C. Eiroa[5], M. C. Wyatt[6], J.-F. Lestrade[10], J. Maldonado[11], D. Rodriguez[12], J. S. Greaves[13], B. Montesinos[14], A. Mora[15], M. Booth[16], G. Duchêne[17,18,19], D. Wilner[20], and J. Horner[21,4]

[1] Space Telescope Science Institute, 3700 San Martin Drive, Baltimore, MD 21218, USA; amaya@stsci.edu
[2] Center for Astrophysical Sciences, Johns Hopkins University, Baltimore MD 21218, USA
[3] School of Physics, University of New South Wales, Sydney, NSW 2052, Australia
[4] Australian Centre for Astrobiology, University of New South Wales, Sydney, NSW 2052, Australia
[5] Departamento Física Teórica, Universidad Autónoma de Madrid, Cantoblanco, E-28049, Madrid, Spain
[6] Institute of Astronomy, University of Cambridge, Madingley Road, Cambridge, CB3 0HA, UK
[7] SRON Netherlands Institute for Space Research, NL-9747 AD, Groningen, Netherlands
[8] Herzberg Astronomy and Astrophysics, National Research Council of Canada, 5071 West Saanich Road, Victoria, BC V9E 2E7, Canada
[9] Department of Physics and Astronomy, University of Victoria, Finnerty Road, Victoria, BC, V8W 3P6, Canada
[10] Observatoire de Paris, CNRS, 61 Avenue de l'Observatoire, F-75014, Paris, France
[11] INAF—Osservatorio Astronomico di Palermo, Piazza Parlamento 1, I-90134 Palermo, Italy
[12] Universidad de Chile, Camino el Observatorio 1515, Las Condes, Santiago, Casilla 36-D, Chile
[13] School of Physics and Astronomy, University of St. Andrews, North Haugh, St. Andrews KY16 9SS, UK
[14] Centro de Astrobiología, CSIC-INTA, ESAC Campus, P.O. Box 78, E-28691 Villanueva de la Cañada, Madrid, Spain
[15] ESA-ESAC, *Gaia* SOC, P.O. Box 78 E-28691 Villanueva de la Cañada, Madrid, Spain
[16] Instituto de Astrofísica, Pontíficia Universidad Católica de Chile, Vicuña Mackenna 4860, 7820436 Macul, Santiago, Chile
[17] Astronomy Department, University of California, Berkeley, CA 94720, USA
[18] Université Grenoble Alpes, IPAG, F-38000 Grenoble, France
[19] CNRS, IPAG, F-38000 Grenoble, France
[20] Harvard–Smithsonian Center for Astrophysics, 60 Garden Street, Cambridge, MA 02138, USA
[21] Computational Engineering and Science Research Centre, University of Southern Queensland, West Street, Toowoomba Qld 4350, Australia
Received 2014 October 15; accepted 2015 January 14; published 2015 March 12

ABSTRACT

The study of the planet–debris disk connection can shed light on the formation and evolution of planetary systems and may help "predict" the presence of planets around stars with certain disk characteristics. In preliminary analyses of subsamples of the *Herschel* DEBRIS and DUNES surveys, Wyatt et al. and Marshall et al. identified a tentative correlation between debris and the presence of low-mass planets. Here we use the cleanest possible sample out of these *Herschel* surveys to assess the presence of such a correlation, discarding stars without known ages, with ages <1 Gyr, and with binary companions <100 AU to rule out possible correlations due to effects other than planet presence. In our resulting subsample of 204 FGK stars, we do not find evidence that debris disks are more common or more dusty around stars harboring high-mass or low-mass planets compared to a control sample without identified planets. There is no evidence either that the characteristic dust temperature of the debris disks around planet-bearing stars is any different from that in debris disks without identified planets, nor that debris disks are more or less common (or more or less dusty) around stars harboring multiple planets compared to single-planet systems. Diverse dynamical histories may account for the lack of correlations. The data show a correlation between the presence of high-mass planets and stellar metallicity, but no correlation between the presence of low-mass planets or debris and stellar metallicity. Comparing the observed cumulative distribution of fractional luminosity to those expected from a Gaussian distribution in logarithmic scale, we find that a distribution centered on the solar system's value fits the data well, while one centered at 10 times this value can be rejected. This is of interest in the context of future terrestrial planet detection and characterization because it indicates that there are good prospects for finding a large number of debris disk systems (i.e., with evidence of harboring planetesimals, the building blocks of planets) with exozodiacal emission low enough to be appropriate targets for an *ATLAST*-type mission to search for biosignatures.

Key words: circumstellar matter – infrared: stars – interplanetary medium – Kuiper Belt: general – planet–disk interactions – planetary systems

1. INTRODUCTION

Planetesimals are the building blocks of planets, and mid- and far-infrared observations with *Spitzer* and *Herschel* indicate that at least 10–25% of mature stars (ages of 10 Myr to 10 Gyr) with a wide range of masses (corresponding to spectral types A–M) harbor planetesimal disks with disk sizes of tens to hundreds AU. This frequency is a lower limit because the surveys are limited by sensitivity. The evidence for planetesimals comes from the presence of infrared emission in excess of that expected from the stellar photosphere, thought to arise from a circumstellar dust disk; because the lifetime of the dust grains (<1 Myr) is much shorter than the age of the star (>10 Myr), it is inferred that the dust cannot be primordial but must be the result of steady or stochastic dust production generated by the collision, disruption, and/or sublimation of planetesimals (for reviews, see Wyatt 2008; Krivov 2010 ; Moro-Martín 2013; Matthews et al. 2014).

The Sun harbors such a debris disk, produced by the asteroids, comets, and Kuiper Belt objects (Jewitt et al. 2009) with a dust production rate that has changed significantly with time, being higher in the past when the asteroid and Kuiper belts (KBs) were more densely populated (Booth et al. 2009). Today, the solar system's debris disk is fainter than the faintest extrasolar debris disks we can observe with *Herschel* (Moro-Martín 2003; Vitense et al. 2012), with a 3σ detection limit at 10–20 times the level of dust in the current KB (Eiroa et al. 2013; B. C. Matthews et al. 2015, in preparation). There is evidence of planetesimals around A- to M-type stars in both single- and multiple-star systems. These stars span several orders of magnitude difference in stellar luminosities, implying that planetesimal formation, a critical step in planet formation, is a robust process that can take place under a wide range of conditions.

It is therefore not surprising that planets and debris disks coexist (Beichman et al. 2005; Moro-Martín et al. 2007b, 2010; Maldonado et al. 2012; Wyatt et al. 2012; Marshall et al. 2014). However, based on *Spitzer* debris disk surveys, no statistical correlation has been found to date between the presence of known high-mass planets and debris disks (Moro-Martín et al. 2007a; Bryden et al. 2009; Kóspál et al. 2009). These studies were focused on high-mass planets ($>30\,M_{\oplus}$) because, at the time, the population of low-mass planets was unknown. Overall, the lack of correlation was understood within the context that the conditions to form debris disks are more easily met than the conditions to form high-mass planets, in which case one would not expect a correlation based on formation conditions; this was also consistent with the studies that showed that there is a correlation between stellar metallicity and the presence of massive planets (Santos et al. 2004; Fisher & Valenti 2005; Maldonado et al. 2012), but there is no correlation between stellar metallicity and the presence of debris disks (Bryden et al. 2006; Greaves et al. 2006; Maldonado et al. 2012).

Recent results from the radial velocity surveys indicate that, similar to debris disks, there is no correlation between the presence of low-mass planets and stellar metallicity (Ghezzi et al. 2010; Mayor et al. 2011; Buchhave et al. 2012). This might indicate that the conditions to form low-mass planets are more easily met than those to form high-mass planets. A natural question to ask is whether low-mass planets and debris disks are correlated.

A correlation between terrestrial planets in the inner region of the planetary systems and cold debris dust has been predicted to exist based on a comprehensive set of dynamical simulations consisting of high-mass planets, embryos, and inner and outer belts of planetesimals. These simulations find a strong correlation between the presence of cold dust and the occurrence of terrestrial planets because systems with cold dust imply a calm dynamical evolution where the building blocks of low-mass planets have been able to grow and survive; on the other hand, systems with dynamically active high-mass planets tend to destroy both the outer dust-producing planetesimal belt and the building blocks of the terrestrial planets (Raymond et al. 2011, 2012).

Herschel observations have opened a new parameter space that allows us to explore fainter and colder debris disks, improving our knowledge of debris disk frequency, in particular around later-type stars. In addition, since the *Spitzer* planet–debris disk correlation studies were carried out, a large number of low-mass planets have been detected, the frequency of which can now be characterized. Tentative detection of a correlation between low-mass planets and debris disks was presented in Wyatt et al. (2012) from a preliminary study based on a *Herschel*–DEBRIS subsample of the nearest 60 G-type stars, which was also seen in the volume-limited sample of radial velocity planet host stars examined by Marshall et al. (2014). In this paper, we revisit the planet–debris disk correlation (or lack thereof) in the *Herschel* DEBRIS and DUNES surveys (Eiroa et al. 2010;2013; Matthews et al. 2010; B. C. Matthews et al. 2015, in preparation) to assess whether the frequency and properties of debris disks around a control sample of stars are statistically different from those around stars with high-mass or low-mass planets. In a companion paper (Marshall et al. 2014), we describe the individual exoplanet host systems, their debris disks, and the disk dependencies on planetary system properties such as planet semimajor axis and eccentricity.

The selection criteria of the different samples used in this study are presented in Section 2 (with a discussion of biases in Section 5). A detailed discussion of the statistical analysis using Kolmogorov–Smirnov (K–S), Fisher's exact, and survival analysis tests can be found in Section 3 (regarding the frequency and properties of debris disks and their dependence on the presence of high-mass and low-mass planets), Section 4 (regarding the correlation with stellar metallicity), and Section 6 (regarding the distribution of the debris disk fractional luminosities). For a summary and discussion of our results the reader is directed to Section 7.

2. SAMPLE SELECTION

Table 1 lists the selection criteria of the different samples of stars used in our statistical analysis. Table 2 gives information on their stellar parameters, and Table 3 lists the observed fluxes and photospheric estimates at 100 μm and the strength of the excess emission. Detailed information on the procedures followed in this paper for source extraction, photosphere subtraction, and SED fitting can be found in Kennedy et al. (2012a, 2012b).

All the stars included in this study are drawn from the *Herschel* DEBRIS and DUNES surveys. DEBRIS is an unbiased volume-limited survey for M-, K-, G-, F-, and A-type stars, where the volume limits are 8.6, 15.6, 21.3, 23.6, and 45.5 pc, respectively (Phillips et al. 2010; Matthews 2010; B. C. Matthews et al. 2015, in preparation). The DUNES survey covers mid-F- to mid-K-type stars within 20 pc (irrespective of planet or debris disk presence), plus a handful of stars within 25 pc known to harbor planets and/or debris disks (Eiroa et al. 2010, 2013).

2.1. Set 1: Control Sample Irrespective of Planet and Debris Disk Presence

To maximize completeness from the DEBRIS and DUNES surveys, we selected for Set 1 all the FGK stars within 20 pc.

The *Spitzer* surveys found that the upper envelope of the 70 μm debris disk emission shows a decline over the ~100 Myr of a star's lifetime (Bryden et al. 2006; Hillenbrand et al. 2008; Carpenter 2009). Therefore, to avoid introducing biases due to stellar age, we further restrict the control sample to stars with ages >100 Myr (of the stars with known ages, only three were excluded because of youth). Our stellar ages are obtained from

Table 1
Sample Description

Set	Description
1	FGK stars in DEBRIS and DUNES with distances <20 pc, ages >100 Myr, and no binary companions at <100 AU
2	Subset from Set 1 without known planets
3	Subset from Set 1 harboring high-mass planets with masses >30 $M_{\oplus}$
	3a: for planets at >0.1 AU
	3b: for planets at 0.1 AU
4	Subset from Set 1 harboring low-mass planets with masses <30 $M_{\oplus}$
5	Subset from Set 1 harboring excess emission at 100 μm, i.e., with $(F_{100} - F_{*,100})/\sigma_{100} > 3$)
6	Subset from Set 1 with single planets
7	Subset from Set1 with multiple planets
1y, 2y, 3ay, 3by, 4y, 5y	Subsets from Sets 1–5 with ages <1 Gyr
1o, 2o, 3ao, 3bo, 4o, 5o	Subsets from Sets 1–5with ages >1 Gyr
1oy, 2oy	Subsets from Sets 1 and 2 with ages 0.1–5 Gyr
1oo, 2oo	Subsets from Sets 1 and 2 with ages >5 Gyr
1l, 2l, 3al, 3bl, 4l, 5l	Subsets from Sets 1–5 with metallicities smaller than the average [Fe/H] $\leqslant -0.12$
1h, 2h, 3ah, 3bh, 4h, 5h	Subsets from Sets 1–5 with metallicities larger than the average [Fe/H] >−0.12
1t, 2t, 3at, 3bt, 4t, 5t	Subsets from Sets 1–5 with estimated dust temperature, assuming a blackbody

Vican et al. (2012) and Eiroa et al. (2013). Stellar ages can be very uncertain, and individual systems may end up in the wrong age bin.[22] However, for a statistical analysis such as the one in this paper, the best approach is to use an age database as "uniform" as possible. Our ages are based on gyrochronology, Ca II chromospheric emission (R'_{HK}), and X-ray flux, always in that order of priority, acknowledging the decreasing reliability of the corresponding age measurements. Gyrochronology ages come from Vican et al. (2012) and are available for 17 stars in our sample; they can be unreliable for young stars (<300 Myr), but out of those 17 stars, only one star is in that age range. When several chromospheric ages are available, we favored the ages in Eiroa et al. (2013) over those in Vican et al. (2012) because the latter were based on a literature search, whereas the former were derived using spectra obtained by the DUNES team and their internally consistent estimates of Ca II activity index (out of the 162 chromospheric ages used, 107 come from Eiroa et al. 2013). Stars without estimated ages were excluded from our analysis.

We do not include A-type stars in this study because the planet searches around these targets are preferentially done around evolved A-type stars (classes III, III–IV, and IV) with lower jitter and narrower absorption lines (Johnson et al. 2011), whereas the A-type stars targeted by DEBRIS are main-sequence (class V). Therefore, we do not have information on planet presence for most A-type stars in the DEBRIS survey. Regarding M-type stars, 89 were observed by DEBRIS, three harboring planets, one of which is also harboring a debris disk (GJ 581—Lestrade et al. 2012). We do not include M-type stars in this study because of low number statistics and because they might probe into a different regime of planetesimal and planet formation than the FGK-type stars.

The DEBRIS and DUNES surveys include single and binary/multiple stars. Previous studies indicate that there are differences in both disk frequency and planet frequency between singles and binaries, and these could introduce a bias in our statistical analysis. Regarding disk frequency, Rodriguez & Zuckerman (2012) found that, out of a sample of 112 main-sequence debris disk stars, 25 ± 4% were binaries, significantly lower than the expected 50% for field stars, with a lack of binary systems at separations of 1–100 AU; for the debris disk hosts in the DEBRIS sample, the multiplicity frequency is ∼28% (D. R. Rodriguez et al. 2015, in preparation). Regarding planet frequency, Eggenberger et al. (2007, 2011) carried out a survey with VLT/NACO to look for stellar companions around 130 nearby solar-type stars and found that the difference in binarity fraction between the nonplanet hosts and the planet hosts is 13.2 ± 5.1% for binary separations <100 AU. In a more recent study, Wang et al. (2014) compared the stellar multiplicity of field stars to that of a sample of 138 bright *Kepler* multiplanet candidate systems, finding also that, for the planet hosts, the binary fraction is significantly lower than field stars for binary semimajor axes <20 AU. An additional observation is that, even within the giant planet regime, binaries tighter than 100 AU show a different distribution of masses, suggesting a different formation mechanism and/or dynamical history (Duchene 2010). In view of all these studies, we have excluded from our samples 96 binary systems with semimajor axis <100 AU to avoid introducing a bias in our analysis. In doing that, we are naturally excluding all circumbinary disks (Kennedy et al. 2012b; D. R. Rodriguez et al. 2015, in preparation), limiting our analysis to those that are circumstellar. This seems appropriate because one would expect that the degree to which the dust is affected by planets (if present) is different, whether the dust is circumbinary or circumstellar, and this could again bias any potential planet–disk correlation.

Differences in infrared background levels could introduce a bias to the debris disk detection; however, both the DUNES and DEBRIS surveys excluded targets that were predicted to be in regions with high contamination from galactic cirrus.[23] In

[22] Comparing, for example, the stellar ages in Sierchio et al. (2014) to those in Vican et al. (2012), among the 48 stars that these two studies have in common, we find that differences in ages are less than 50%, except for five stars: HD126660/HIP 70497 (80%), HD23754/HIP 17651(83%), HD189245/HIP 98470 (733%), HD20630/HIP 15457 (70%), and HD101501/HIP 56997 (84%). The age estimations are therefore broadly consistent.

[23] The unconfirmed planet host star α Cen B was observed as part of the DUNES and *Hi-Gal* programs, but it was excluded from this analysis because its high background level does not fulfill the DUNES and DEBRIS selection criteria, and our analysis is intended to be unbiased.

Table 2
Stellar Properties

HIP	HD	GJ	UNS	Survey	d (pc)	SpT	$T_{\rm eff}$ (K)	[Fe/H] (dex)	$L_{\rm bol}$ ($L_\odot$)	Age (Gyr)	Binary Sep.[a] (AU)
544	166	5	G030A	DUNES	13.68	G8 V	5512	0.15	0.631	0.17	⋯
910	693	10	F069A	DUNES	18.74	F8 V Fe-0.8 CH-0.5	6235	−0.32	3.280	3.04	⋯
1368	⋯	14	K115A	DEBRIS	14.99	K7	4089	**	0.109	**	⋯
1599	1581	17	F005A	DEBRIS	8.59	F9.5 V	6013	−0.29	1.288	4.03	⋯
3093	3651	27	K045A	DUNES	11.06	K0 V	5261	0.2	0.515	6.43	A-B: 474
3583	4391	1021	G041A	DEBRIS	15.17	G5 V Fe-0.8	5845	−0.2	0.974	0.84	A-B: 252
	⋯	146.01	G041B	DEBRIS	15.17	G5 V Fe-0.8	4228	**	0.019	0.84	A-B: 252
3765	4628	33	K016A	DEBRIS	7.45	K2.5 V	5006	−0.24	0.293	5.31	⋯
3821	4614	34A	G004A	DUNES	5.95	F9V-G0V	5932	−0.23	1.209	6.43	⋯
3821	4614	34B	G004B	DUNES	5.95	F9V-G0V	5932	−0.23	1.209	6.43	⋯
3909	4813	37	F038A	DUNES	15.75	F7 V	6260	−0.16	1.770	2.93	⋯
4022	4967	40A	K127A	DEBRIS	15.61	K6 V k	4136	**	0.109	1.34	A-B: 262
	⋯	40B	K127B	DEBRIS	15.61	K5	2541	**	0.001	1.34	A-B: 262
4148	5133	42	K089A	DUNES	14.16	K2.5 V (k)	4913	−0.16	0.292	3.64	⋯
5862	7570	55	F032A	DEBRIS	15.12	F9 V Fe+0.4	6144	0.17	1.950	4.12	⋯
7235	9540	59A	G092A	DEBRIS	19.03	G8.5 V	5453	0.01	0.540	2.20	⋯
7513	9826	61	F020A	DUNES	13.49	F8V	6224	0.11	3.446	7.26	⋯
7978	10647	3109	F051A	DUNES	17.43	F9 V	6181	−0.09	1.571	1.74	⋯
8102	10700	71	G002A	GT	3.65	G8.5 V	5421	−0.43	0.501	5.82	⋯
8768	11507	79	K043A	DUNES	11.02	K7	3967	**	0.080	0.67	⋯
10798	14412	95	G024A	DUNES	12.67	G8 V	5479	−0.46	0.431	6.54	⋯
11452	15285	98	⋯	DUNES	17.14	K5V-M1.5 V	3921	⋯	0.210	⋯	⋯
11964	16157	103	⋯	DUNES	11.60	K6Ve-M0VP	3790	⋯	0.092	0.18	⋯
12653	17051	108	F046A	DEBRIS	17.17	F9 V Fe+0.3	6158	0.07	1.690	1.52	⋯
12777	16895	107A	F010A	DUNES	11.13	F7V-F8V	6314	0.03	2.250	7.92	⋯
12777	16895	107B	F010B	DUNES	11.13	F7V-F8V	6314	0.03	2.250	7.92	⋯
12843	17206	111	F024A	DEBRIS	14.24	F6 V	6435	0.04	2.712	0.71	⋯
13375	⋯	116	K108A	DEBRIS	14.76	K5	4006	**	0.058	**	⋯
14445	19305	123	K107A	DEBRIS	14.75	K5	3999	**	0.101	0.00	⋯
15371	20807	138	G018A	DUNES	12.02	G0 V	5922	−0.16	1.009	3.59	A-B: 3717
15457	20630	137	G011A	DEBRIS	9.14	G5 V	5738	0.09	0.846	0.68	⋯
15510	20794	139	G005A	DEBRIS	6.04	G8 V	5500	−0.34	0.663	6.56	⋯
15799	21175	3222	⋯	DUNES	17.42	K0V-K1V	5087	0.12	0.535	2.84	⋯
15919	21197	141	K122A	DEBRIS	15.39	K4 V	4534	**	0.220	1.14	⋯
16134	21531	142	K061A	DUNES	12.51	K6 V k	4172	−0.13	0.126	1.21	⋯
16537	22049	144	K001A	GT	3.22	K2 V (k)	5100	−0.11	0.337	1.28	⋯
16711	22496	146	K079A	DEBRIS	13.59	K5.0	4194	**	0.121	0.97	⋯
16852	22484	147	F022A	DEBRIS	13.98	F8 V	6031	−0.07	3.203	7.59	⋯
17420	23356	⋯	K087A	DUNES	13.95	K2.5 V	4982	−0.12	0.299	7.35	⋯
17439	23484	152	⋯	DUNES	16.03	K1V-K2V	5166	0.05	0.402	0.76	⋯
17651	23754	155	F053A	DEBRIS	17.61	F5 IV-V	6646	0.07	5.158	1.83	⋯
18280	⋯	156	K124A	DEBRIS	15.52	K7	4121	**	0.114	0.78	⋯
19884	27274	167	K067A	DUNES	13.05	K4.5 V (k)	4529	0.06	0.195	0.00	⋯
22263	30495	177	G029A	DUNES	13.27	G1.5 V CH-0.5	5830	0.04	0.972	0.55	⋯
22449	30652	178	F003A	DEBRIS	8.07	F6V	6538	−0.01	2.870	3.04	⋯
23311	32147	183	K024A	DUNES	8.71	K3 + V	4755	0.29	0.283	10.91	⋯
23693	33262	189	F012A	DEBRIS	11.64	F6V	6213	−0.15	1.496	0.57	A-B: 3743
25544	36435	204.1	G095A	DEBRIS	19.20	G9 V	5473	0.06	0.535	0.40	⋯
26394	39091	9189	G085A	DEBRIS	18.32	G0 V	6000	0.1	1.537	6.04	⋯
27072	38393	216A	F006A	DEBRIS	8.93	F6.5 V	6374	−0.09	2.415	3.45	A-B: 860
	38392	216B	F006B	DEBRIS	8.93	F9 V Fe-1.4 CH-0.7	4905	**	0.290	3.45	A-B: 860
27188	⋯	215	K082A	DEBRIS	13.72	K7	4016	**	0.096	**	⋯
27887	40307	⋯	K065A	DUNES	13.00	K2.5 V	4844	−0.45	0.257	2.60	⋯
28103	40136	225	F028	DUNES	14.88	F0IV-F2V	7000	−0.11	5.562	0.64	⋯
28442	40887	225.2	⋯	DUNES	16.39	K5V-K6.5 V	4330	⋯	0.290	⋯	⋯
29568	43162	3389	G056A	DUNES	16.72	G6.5 V	5582	0	0.711	0.28	A-B: 411
32439	46588	240.1	F056A	DUNES	17.88	F8 V	6244	−0.03	1.785	7.05	⋯
32480	48682	245	F044A	DUNES	16.71	F9 V	6078	0.16	1.870	6.32	⋯
33277	50692	252	G065A	DUNES	17.24	G0 V	5924	−0.11	1.280	5.45	⋯
34017	52711	262	G093A	DUNES	19.16	G0 V	5915	−0.14	1.331	5.54	⋯
34052	53680	264	G059C	DUNES	16.94	G0 V	4314	**	0.145	6.24	A-C: 3134
34065	53705	264.1A	G059A	DUNES	16.94	G0 V	5826	−0.39	1.490	6.24	A-B: 357
34069	53706	264.1B	G059B	DUNES	16.94	G0 V	5314	−0.23	0.492	6.79	A-B: 357

Table 2
(Continued)

HIP	HD	GJ	UNS	Survey	d (pc)	SpT	$T_{\rm eff}$ (K)	[Fe/H] (dex)	$L_{\rm bol}$ ($L_\odot$)	Age (Gyr)	Binary Sep.[a] (AU)
35136	55575	1095	F045A	DUNES	16.89	F9 V	5926	−0.36	1.497	5.25	⋯
37288	⋯	281	K099A	DEBRIS	14.53	K7	4054	**	0.073	2.20	⋯
37349	61606	282A	K090A	DEBRIS	14.19	K3- V	4876	0.06	0.294	0.46	A-B: 827
	⋯	282B	K090B	DEBRIS	14.19	K3- V	4074	**	0.102	0.46	A-B: 827
38784	62613	290	G062A	DUNES	17.18	G8V	5598	−0.08	0.629	3.75	⋯
40693	69830	302	G022A	DUNES	12.49	G8 + V	5419	0.14	0.599	6.43	⋯
40702	71243	305	F077A	DEBRIS	19.57	F5 V Fe-0.8	6702	−0.25	7.467	0.25	⋯
40843	69897	303	F061A	DUNES	18.27	F6 V	6324	−0.39	2.507	4.27	⋯
42438	72905	311	G036A	DUNES	14.36	G1.5Vb	5885	−0.02	0.999	0.27	⋯
42748	⋯	319A&B	K121AB	DEBRIS	15.37	K7	3778	**	0.083	**	A-B: 1758
43587	75732	324A	K060A	DUNES	12.46	K0 IV-V	5283	0.19	0.608	8.43	A-B: 1055
	⋯	324B	K060B	DUNES	12.46	K0 IV-V	2939	**	0.008	8.43	A-B: 1055
43726	76151	327	G068A	DUNES	17.39	G3 V	5815	0.23	1.028	1.65	⋯
44248	76943	332A&B	F040AB	DEBRIS	16.06	F5 IV-V	6569	0.08	5.456	0.83	A-B: 455
44722	⋯	334	K097A	DEBRIS	14.47	K7	3858	**	0.081	1.00	⋯
44897	78366	334.2	G094A	DUNES	19.18	G0 IV-V	6022	0.03	1.301	1.20	⋯
45343	79210	338A	K011A	DEBRIS	6.11	K7	3957	**	0.062	0.70	A-B: 106.7
120005	79211	338B	K011B	DEBRIS	6.11	K7	3864	−0.4	0.068	1.01	A-B: 106.7
46580	82106	349	K064A	DUNES	12.89	K3 V	4781	−0.44	0.231	0.61	⋯
47592	84117	364	F031A	DUNES	15.01	F8 V	6213	−0.21	2.018	4.14	⋯
48113	84737	368	G086A	DEBRIS	18.34	G0 IV-V	5968	0.1	2.629	7.39	⋯
49081	86728	376	G040A	DUNES	15.05	G4 V	5796	0.19	1.369	6.02	⋯
49908	88230	380	K005A	DUNES	4.87	K5	4090	−0.16	0.103	6.60	⋯
53721	95128	407	G033A	DUNES	14.06	G0V	5921	−0.03	1.644	4.93	⋯
54646	97101	414A	K056A	DUNES	11.96	K7 V	4468	−1.5	0.146	4.11	A-B: 408
	⋯	414B	K056B	DUNES	11.96	K7 V	3483	**	0.051	4.11	A-B: 408
55846	99491	429A	G079A	DEBRIS	17.78	G6/8 III/IV	5433	**	0.735	3.79	A-B: 504
55848	99492	429B	G079B	DEBRIS	17.78	G6/8 III/IV	4942	**	0.325	3.79	A-B: 504
56452	100623	432A	K029A	DUNES	9.56	K0- V	5244	−0.38	0.364	4.90	A-B: 162.5
	⋯	432B	K029B	DUNES	9.56	K0- V	9506	**	0.000	4.90	A-B: 162.5
56997	101501	434	G013A	DEBRIS	9.60	G8 V	5555	0.01	0.621	1.66	⋯
56998	101581	435	K059A	DEBRIS	12.40	K4.5 V (k)	4557	**	0.152	0.73	⋯
57443	102365	442A	G012A	DEBRIS	9.22	G2 V	5671	−0.37	0.839	5.80	A-B: 211
	⋯	442B	G012B	DEBRIS	9.22	G2 V	2700	**	0.003	5.80	A-B: 211
57507	102438	446	G069A	DUNES	17.47	G6 V	5618	−0.28	0.699	5.20	⋯
57757	102870	449	F009A	DEBRIS	10.93	F9 V	6130	0.09	3.594	6.41	⋯
57939	103095	451A	K028A	DUNES	9.08	K1 V Fe-1.5	5167	−1.12	0.223	4.61	⋯
58345	103932	453	K034A	DUNES	10.16	K4 + V	4568	0.16	0.212	0.44	⋯
59199	105452	455.3	F030A	DEBRIS	14.94	F1 V	7053	−0.13	4.530	0.68	⋯
61094	⋯	471	K081A	DEBRIS	13.68	K7	3882	**	0.062	**	⋯
61174	109085	471.2	F063A	DEBRIS	18.28	F2 V	6953	−0.02	5.092	2.47	⋯
61317	109358	475	G007AB	DEBRIS	8.44	G0 V	5929	−0.2	1.243	3.96	⋯
61901	110315	481	K092A	DEBRIS	14.19	K4.5 V	4448	**	0.190	6.66	⋯
62207	110897	484	F050A	DUNES	17.37	F9 V Fe-0.3	5939	−0.53	1.098	6.24	⋯
62523	111395	486.1	G057A	DUNES	16.94	G7 V	5647	0.22	0.767	0.37	⋯
62687	111631	488	K036A	DEBRIS	10.60	K7	4073	**	0.093	0.68	⋯
64394	114710	502	G010A	DEBRIS	9.13	G0V	6072	0.11	1.418	1.83	⋯
64792	115383	504	G073A	DUNES	17.56	G0Vs	6043	0.24	2.187	0.16	A-B: 602
64924	115617	506	G008A	DEBRIS	8.55	G7 V	5597	0	0.836	4.58	⋯
65026	115953	508	⋯	DUNES	10.71	K0, M0V-M3V	3752	⋯	0.120	6.00	⋯
65352	116442	3781A	G050A	DEBRIS	15.79	G9 V	5248	−0.14	0.366	7.81	A-B: 416
65355	116443	3782B	G050B	DEBRIS	15.79	G9 V	5036	−0.11	0.289	8.43	A-B: 416
65721	117176	512.1	⋯	DUNES	17.99	G4V-G5V	5513	−0.07	2.989	7.89	⋯
66459	⋯	519	K041A	DEBRIS	10.93	K5	3986	**	0.063	8.01	⋯
66675	118926	521.1	K109A	DEBRIS	14.76	K5	3876	**	0.066	**	⋯
67090	⋯	525	K070A	DEBRIS	13.19	K5	3852	**	0.047	1.00	⋯
67275	120136	527A	F036A	DUNES	15.62	F7V	6826	0.26	3.018	0.47	A-B: 125.1
67275	⋯	527B	F036B	DUNES	15.62	F7V	3580	**	0.032	0.47	A-B: 125.1
67308	120036	1177A	K103A	DEBRIS	14.63	K6.5 V (k)	4116	**	0.115	8.30	A-B: 132.0
67308	⋯	1177B	K103B	DEBRIS	14.63	K6.5 V (k)	4113	**	0.103	8.30	A-B: 132.0
67487	120467	529	K095A	DEBRIS	14.29	K5.5 V (k)	4293	**	0.169	2.28	⋯
67691	234078	532	K091A	DEBRIS	14.19	K5	4169	**	0.111	6.36	⋯
68184	122064	⋯	K032A	DUNES	10.06	K3V	4818	0.1	0.287	3.34	⋯

Table 2
(Continued)

HIP	HD	GJ	UNS	Survey	d (pc)	SpT	$T_{\rm eff}$ (K)	[Fe/H] (dex)	$L_{\rm bol}$ ($L_\odot$)	Age (Gyr)	Binary Sep.[a] (AU)
70218	⋯	546	K096A	DEBRIS	14.39	K6 V	4220	**	0.129	0.40	⋯
70319	126053	547	G063A	DUNES	17.19	G1.5 V	5753	−0.27	0.820	5.80	⋯
70497	126660	549A	F026A	DEBRIS	14.53	F7V	6328	−0.08	4.242	1.08	A-B: 1005
	⋯	549B	F026B	DEBRIS	14.53	F7V	3455	**	0.021	1.08	A-B: 1005
71181	128165	556	K072A	DUNES	13.22	K3V	4769	−0.09	0.240	11.19	⋯
71284	128167	557	F039A	DEBRIS	15.83	F3Vwvar	6889	**	3.557	4.78	⋯
71908	128898	560A	A010A	DUNES	16.57	A7p-F1Vp	7645	⋯	11.263	⋯	⋯
	128898	560B	A010B	DUNES	16.57	⋯		⋯		⋯	⋯
71957	129502	9491	F062A	DEBRIS	18.28	F2 V	6759	0.01	7.474	1.11	⋯
73182	131976	570B	K008B	DUNES	5.86	K4 V	3568	−0.24	0.069	1.36	A-BC: 141.8
73184	131977	570A	K008A	DUNES	5.86	K4 V	4607	0.1	0.210	1.36	A-BC: 141.8
73996	134083	578	F076A	DUNES	19.55	F5 V	6646	0.05	3.322	3.95	⋯
75277	136923	⋯	G101A	DEBRIS	19.60	G9 V	5369	**	0.497	4.81	⋯
76779	139763	⋯	K126A	DEBRIS	15.56	K6 V k	4161	**	0.114	2.93	⋯
77257	141004	598	G019A	DEBRIS	12.12	G0 IV-V	5967	0.06	2.126	5.49	⋯
77760	142373	602	G052A	DEBRIS	15.89	G0 V Fe-0.8...	5897	−0.5	3.195	7.39	⋯
78072	142860	603	F011A	DEBRIS	11.26	F7V	6387	−0.17	3.097	3.49	⋯
78459	143761	606.2	G064A	DUNES	17.24	G0 V	5858	−0.17	1.780	7.33	⋯
78775	144579	611A	K098A	DUNES	14.51	K0 V Fe-1.2	5330	−0.6	0.439	6.04	A-B: 1020
	⋯	611B	K098B	DUNES	14.51	K0 V Fe-1.2	3372	**	0.003	6.04	A-B: 1020
79248	145675	614	⋯	DUNES	17.57	K0IV-K0V	5336	0.43	0.653	7.45	⋯
79755	147379	617A	K039A	DEBRIS	10.80	K7	4082	**	0.097	1.01	A-B: 697
79762	⋯	617B	K039B	DEBRIS	10.80	K7	3345	**	0.029	1.01	A-B: 697
80725	148653	⋯	⋯	DUNES	19.66	K1V-K2V	5040	⋯	0.636	1.89	⋯
82003	151288	638	K031A	DEBRIS	9.81	K5	4418	**	0.125	7.67	⋯
83389	154345	651	G088A	DUNES	18.58	G8V	5485	−0.06	0.619	3.84	⋯
83990	154577	656	K080A	DEBRIS	13.63	K2.5 V (k)	4920	−0.64	0.221	8.09	⋯
84862	157214	672	G035A	DUNES	14.33	G0V	5776	−0.41	1.281	5.91	⋯
85235	158633	675	K062A	DUNES	12.80	K0V	5334	−0.44	0.417	5.31	⋯
85295	157881	673	K021A	DUNES	7.70	K5	4201	−0.03	0.115	2.20	⋯
86796	160691	691	G047	DUNES	15.51	G3V/VI-G5V	5787	0.29	1.821	>1	⋯
88601	165341	702A	K007A	DUNES	5.08	K0V	5312	0.05	0.594	1.05	⋯
88601	165341	702A	K007B	DUNES	5.08	K0V	5312	0.05	0.594	1.05	⋯
88972	166620	706	K044A	DUNES	11.02	K2 V	5047	−0.07	0.346	6.43	⋯
89042	165499	705.1	G075A	DUNES	17.62	G0 V	5953	0.09	1.715	5.40	⋯
89211	166348	707	K068A	DEBRIS	13.13	K6 V (k)	4225	**	0.126	6.04	⋯
91009	234677	719	⋯	DUNES	16.35	K4V-K6V	4200	0.05	0.232	0.12	⋯
92043	173667	725.2	F073	DUNES	19.21	F5V-F7IV	6431	0.04	6.141	4.74	⋯
95149	181321	755	G091A	DEBRIS	18.83	G1 V	5793	−0.21	0.791	0.15	⋯
95995	184467	762.1	⋯	DUNES	16.96	K1V-2 V	5027	−0.22	0.682	7.48	⋯
96100	185144	764	G003	DUNES	5.75	G9V-K0V	5276	−0.18	0.427	3.67	⋯
97944	188088	770	⋯	DUNES	14.05	K2V/VI-K4V	4687	−0.2	0.770	0.49	⋯
98698	190007	775	K063A	DEBRIS	12.86	K4 V (k)	4555	**	0.219	0.59	⋯
98959	189567	776	G077A	DUNES	17.73	G2 V	5764	−0.22	1.024	4.06	⋯
99240	190248	780	⋯	DUNES	6.11	G8IV	5597	0.3	1.246	8.30	⋯
99701	191849	784	K012A	DEBRIS	6.20	K7.0	3881	**	0.060	0.85	⋯
99825	192310	785	K027A	DEBRIS	8.91	K2 + V	5096	0.09	0.406	7.50	⋯
100925	194640	790	G098A	DEBRIS	19.52	G8 V	5574	0.06	0.766	4.78	⋯
101955	196795	795	⋯	DUNES	16.72	K5V-M0/1 V	4181	⋯	0.331	1.20	⋯
101997	196761	796	G037A	DUNES	14.38	G8 V	5486	−0.3	0.540	5.63	⋯
102186	196877	798	K057A	DEBRIS	12.15	K5.0	4167	**	0.083	0.49	⋯
102485	197692	805	F027A	DEBRIS	14.68	F5 V	6640	0.03	3.907	0.31	⋯
104092	200779	818	K116A	DEBRIS	15.10	K6 V	4310	**	0.167	1.12	⋯
104214	201091	820A	K002A	DUNES	3.49	K5V	4394	−0.25	0.144	6.18	⋯
104217	201092	820B	K002B	DUNES	3.50	K7V-M0V	4002	−0.39	0.092	8.45	⋯
104440	⋯	818.1 C	F079C	DEBRIS	19.81	F9.5 V	3370	**	0.008	0.69	AB-C: 142.6
105090	202560	825	K004A	DEBRIS	3.95	K7.0	3912	**	0.072	2.56	⋯
105858	203608	827	F007A	DEBRIS	9.26	F9.5 V	6213	−0.84	1.522	0.57	⋯
106696	205390	833	K101A	DUNES	14.62	K1.5 V	5013	−0.2	0.305	2.01	⋯
107350	206860	836.7	G080A	DUNES	17.88	G0 V CH-0.5	5992	−0.2	1.128	0.32	A-B: 772
107649	207129	838	G053A	DUNES	16.00	G0 V Fe+0.4	5969	−0.06	1.282	6.98	A-B: 880
108870	209100	845	K003A	DUNES	3.62	K4 V (k)	4672	−0.06	0.210	0.90	A-BC: 1456
109422	210302	849.1	F064A	DUNES	18.28	F6 V	6463	0.09	2.883	3.53	⋯

Table 2
(Continued)

HIP	HD	GJ	UNS	Survey	d (pc)	SpT	$T_{\rm eff}$ (K)	[Fe/H] (dex)	$L_{\rm bol}$ ($L_\odot$)	Age (Gyr)	Binary Sep.[a] (AU)
110443	211970	1267	K076A	DEBRIS	13.53	K5.0	4020	**	0.085	3.78	⋯
111960	214749	868	K077A	DEBRIS	13.55	K4.5 V k	4480	**	0.182	3.96	⋯
112447	215648	872A	F043A	DEBRIS	16.30	F7V	6188	−0.2	4.780	7.91	A-B: 192.3
	⋯	872B	F043B	DEBRIS	16.30	F7V	3370	**	0.024	7.91	A-B: 192.3
112774	216133	875	K088A	DEBRIS	14.13	K7	3854	**	0.056	0.55	⋯
113283	216803	879	K019A	DEBRIS	7.61	K4 + V k	4578	**	0.187	0.38	A-B: 53498
113421	217107	⋯	G102AB	DEBRIS	19.86	G8 IV-V	5645	0.27	1.173	8.09	⋯
113576	217357	884	K022A	DUNES	8.21	K5	4079	−1.5	0.091	4.90	⋯
114361	218511	1279	K114A	DEBRIS	14.99	K5.5 V (k)	4369	**	0.153	1.26	⋯
116215	221503	898	K112A	DEBRIS	14.90	K5	4214	**	0.132	8.07	A-BC: 5047
116745	222237	902	K052A	DUNES	11.41	K3 + V	4743	−0.24	0.221	6.60	⋯
116763	222335	902.1	G087A	DEBRIS	18.58	G9.5 V	5285	−0.14	0.439	2.31	⋯
116771	222368	904	F021A	DEBRIS	13.72	F7V	6227	−0.13	3.512	6.22	⋯
120005	79211	338B	K011B	DEBRIS	6.11	K7	3864	−0.4	0.068	1.01	A-B: 106.7
	26976	166B&C	K006BC	DUNES	4.98	K0.5 V	3283	**	0.008	4.30	AB-C: 413

Note.
[a] Projected binary separation from D. R. Rodriguez et al. (2015, in preparation).

addition, all the targets in Set 1 have been inspected to exclude, to the best of our knowledge, sources subject to confusion.

The total number of stars in Set 1 (FGK stars within 20 pc, ages >100 Myr and no binary companions at <100 AU) is 204. All the other star samples discussed in the subsections below are extracted from Set 1, i.e., they fulfill the same criteria with respect to stellar type, distance, age, absence of close binary companions, and nearby confusion.

Table 4 lists the planetary systems found within Set 1. There are 22 stars harboring planets and an additional three with unconfirmed planetary systems, namely HD 22049 (ϵ Eri), HD 10700 (τ Cet), and HD 189567.

Even though the targets are located at a range of distances (see Figure 1), we do not expect this to introduce a significant bias to the planet–debris disk correlation study presented in this paper for the following reasons. Regarding planet detection, the Doppler studies do not depend on distance (although their sensitivity depends on V magnitude and spectral type, and this may account for the closer distances of stars hosting low-mass planets only). Regarding debris disk detection, (a) the DUNES observations are designed to always reach the stellar photosphere at 100 μm to a uniform signal-to-noise ratio >5; (b) we assess the planet–debris correlation using survival analysis that takes into account the upper limits from the DEBRIS survey; and (c) we use a distance-independent variable, the dust excess flux ratio $(F_{\rm obs}^{100} - F_{\rm star}^{100})/F_{\rm star}^{100}$, where $F_{\rm obs}^{100}$ is the observed flux at 100 μm, and $F_{\rm star}^{100}$ is the expected photospheric value at that wavelength.

2.2. Set 2: No-planet Sample

Set 2 is the subset of stars from Set 1 without known planets, as of 2014 August. The number of stars in this set is 182 (179 if including the three unconfirmed planetary systems).

2.3. Set 3: High-mass Planet Sample

Set 3 is the subset of stars from Set 1 known as of 2014 August to harbor one or more planets with masses >30 $M_\oplus$ (>0.094 $M_{\rm Jup}$). We call this the high-mass planet sample. The planetary system properties are listed in Table 4. The number of stars in this set is 16 (17 if including the three unconfirmed planetary systems). Note that some of these systems also harbor low-mass planets. We chose this limiting planet mass because for stars harboring planets >30 $M_\oplus$, there is a correlation between the presence of planets and stellar metallicity (Santos et al. 2004; Fisher & Valenti 2005). On the other hand, for stars harboring planets <30 $M_\oplus$, there is no correlation between the presence of planets and stellar metallicity (Ghezzi et al. 2010; Mayor et al. 2011). This might indicate differences in the planet formation mechanism that may affect the planet–debris disk correlation. We further divide this set into two subsets: 3a (for planets with $a > 0.1$ AU) and 3b (for planets with $a < 0.1$ AU).

2.4. Set 4: Low-mass Planet Sample

Set 4 is the subset of stars from Set 1 known as of August 2014 to harbor one or more planets with masses <30 $M_\oplus$ and no higher-mass planets. We call this the low-mass planet sample. There are six stars in this set (eight if including the three unconfirmed planetary systems).

2.5. Set 5: Debris Disk Sample

Due to the wavelength coverage of the DUNES and DEBRIS surveys[24], this study is focused on the 100 μm emission. Set 5 is the subset of 29 stars from Set 1 with debris disks detected by *Herschel* at 100 μm, i.e., stars for which signal to noise ratio of the excess emission, ${\rm SNR}_{\rm dust} > 3$, where ${\rm SNR}_{\rm dust} = \frac{F_{\rm obs}^{100} - F_{\rm star}^{100}}{\sqrt{\sigma_{\rm obs}^{100\,2} + \sigma_{\rm star}^{100\,2}}}$, and $F_{\rm obs}^{100}$ and $F_{\rm star}^{100}$ are the observed flux at 100 μm and the estimated photospheric flux, respectively, whereas $\sigma_{\rm obs}^{100}$ and $\sigma_{\rm star}^{100}$ are their 1σ uncertainties. The 70 μm *Spitzer* observations do not identify any additional debris disks within Set 1. This indicates that the 100 μm

[24] DEBRIS and DUNES utilized the simultaneous 100 and 160 μm imaging mode as the basis for their survey data, with both teams taking additional data toward selected sources using the 70 and 160 μm imaging mode of PACS and 250, 350, and 500 μm imaging with SPIRE as appropriate.

Table 3
Observed Fluxes and Excess Properties

HIP	HD	GJ	UNS	F_{obs}^{100a} (mJy)	F_{star}^{100b} (mJy)	$F_{obs}^{100}/\sigma_{obs}^{100c}$	$F_{obs}^{100}/F_{star}^{100d}$	$F_{dust}^{100}/F_{star}^{100d}$	L_{dust}/L_{star}^{e}	SNR_{dust}[f]	Dust Detec.?	Set[g]
544	166	5	G030A	63.55 ± 4.45	7.54 ± 0.13	14.28	8.43	7.43	6.49E-05	12.58	Y	1,2,5
910	693	10	F069A	19.29 ± 2.52	14.41 ± 0.33	7.65	1.34	0.34	<2.57E-06	1.92	N	1,2
1368	⋯	14	K115A	41.27 ± 6.55	2.85 ± 0.07	6.30	14.46	13.46	9.50E-05	5.86	Y	1,2,5, (conf.?)
1599	1581	17	F005A	34.64 ± 2.72	30.07 ± 0.52	12.75	1.15	0.15	<1.40E-06	1.65	N	1,2
3093	3651	27	K045A	6.61 ± 1.49	10.82 ± 0.21	4.42	0.61	−0.39	<1.23E-07	−2.79	N	1,3a,6
3583	4391	1021	G041A	11.12 ± 2.25	8.05 ± 0.11	4.94	1.38	0.38	<4.40E-06	1.36	N	1,2
	⋯	146.01	G041B	−1.70 ± 2.17	0.42 ± 0.04	−0.79	<15.41	<14.41	<1.37E-04	−0.98	N	1,2
3765	4628	33	K016A	15.16 ± 2.88	16.41 ± 0.27	5.26	0.92	−0.08	<2.58E-06	−0.43	N	1,2
3821	4614	34A	G004A	58.96 ± 3.91	74.33 ± 1.54	15.06	0.79	−0.21	<-1.68E-07	−3.65	N	1,2
3821	4614	34B	G004B	10.98 ± 2.10	18.21 ± 0.35	5.22	0.60	−0.40	<-1.74E-07	−3.39	N	1,2
3909	4813	37	F038A	13.31 ± 1.62	10.87 ± 0.25	8.22	1.22	0.22	<1.97E-06	1.49	N	1,2
4022	4967	40A	K127A	−0.63 ± 2.25	2.47 ± 0.05	−0.28	<2.74	<1.74	<1.76E-05	−1.37	N	1,2
	⋯	40B	K127B	−3.35 ± 1.70	0.08 ± 0.00	−1.97	<63.61	<62.61	<2.71E-03	−2.01	N	1,2
4148	5133	42	K089A	13.93 ± 1.56	4.70 ± 0.07	8.91	2.96	1.96	9.99E-06	5.90	Y	1,2,5
5862	7570	55	F032A	23.11 ± 2.49	13.79 ± 0.25	9.29	1.68	0.68	8.83E-06	3.73	Y	1,2,5
7235	9540	59A	G092A	6.15 ± 2.26	3.44 ± 0.05	2.72	<3.76	<2.76	<1.22E-05	1.20	N	1,2
7513	9826	61	F020A	34.09 ± 2.68	29.41 ± 0.52	12.74	1.16	0.16	<1.29E-06	1.72	N	1,3a,7
7978	10647	3109	F051A	825.41 ± 81.22	8.19 ± 0.22	10.16	100.79	99.79	3.11E-04	10.06	Y	1,3a,5,6
8102	10700	71	G002A	190.00 ± 19.00	81.00 ± 1.57	10.00	2.35	1.35	8.70E-06	5.72	Y	1,2,5, (4?,7?)
8768	11507	79	K043A	3.56 ± 1.23	4.15 ± 0.18	2.89	<1.75	<0.75	<8.62E-06	−0.47	N	1,2
10798	14412	95	G024A	6.63 ± 0.97	6.13 ± 0.09	6.83	1.08	0.08	<2.44E-06	0.51	N	1,2
11452	15285	98	⋯	4.27 ± 0.73	4.52 ± 0.06	5.84	0.95	−0.05	<5.12E-06	−0.34	N	1,2
11964	16157	103	⋯	4.11 ± 0.78	5.95 ± 0.14	5.30	0.69	−0.31	<1.09E-06	−2.33	N	1,2
12653	17051	108	F046A	5.76 ± 2.68	9.19 ± 0.17	2.15	<1.50	<0.50	<1.55E-06	−1.28	N	1,3a,6
12777	16895	107A	F010A	25.27 ± 2.36	29.96 ± 0.69	10.70	0.84	−0.16	<2.29E-07	−1.90	N	1,2
12777	16895	107B	F010B	1.84 ± 1.88	3.00 ± 0.26	0.98	<2.49	<1.49	<4.26E-06	−0.61	N	1,2
12843	17206	111	F024A	20.05 ± 2.87	18.80 ± 0.33	6.99	1.07	0.07	<1.42E-06	0.43	N	1,2
13375	⋯	116	K108A	−1.44 ± 1.97	1.68 ± 0.03	−0.73	<3.52	<2.52	<2.81E-05	−1.58	N	1,2
14445	19305	123	K107A	4.26 ± 1.67	2.87 ± 0.06	2.55	<3.24	<2.24	<2.51E-05	0.83	N	1,2
15371	20807	138	G018A	14.48 ± 1.42	12.58 ± 0.22	10.19	1.15	0.15	<1.70E-06	1.32	N	1,2, (conf.?)
15457	20630	137	G011A	23.23 ± 2.28	20.11 ± 0.35	10.21	1.15	0.15	<1.88E-06	1.35	N	1,2
15510	20794	139	G005A	54.45 ± 3.25	40.93 ± 0.77	16.75	1.33	0.33	1.73E-06	4.05	Y	1,4,5,7
15799	21175	3222	⋯	5.18 ± 0.77	5.24 ± 0.07	6.69	0.99	−0.01	<2.36E-06	−0.08	N	1,2
15919	21197	141	K122A	2.75 ± 2.33	3.77 ± 0.06	1.18	<2.59	<1.59	<1.22E-05	−0.44	N	1,2
16134	21531	142	K061A	3.42 ± 1.06	4.37 ± 0.08	3.24	0.78	−0.22	<5.02E-06	−0.89	N	1,2
16537	22049	144	K001A	2000.00 ± 200.00	91.99 ± 1.00	10.00	21.74	20.74	1.30E-04	9.54	Y	1,2,5(3a?,6?)
16711	22496	146	K079A	6.32 ± 2.35	3.49 ± 0.08	2.69	<3.83	<2.83	<2.75E-05	1.20	N	1,2
16852	22484	147	F022A	73.24 ± 7.31	27.97 ± 0.47	10.02	2.62	1.62	1.01E-05	6.18	Y	1,2,5
17420	23356	⋯	K087A	15.12 ± 1.30	4.71 ± 0.07	11.59	3.21	2.21	1.35E-05	7.97	Y	1,2,5
17439	23484	152	⋯	90.03 ± 5.41	4.22 ± 0.05	16.65	21.33	20.33	7.00E-05	15.87	Y	1,2,5
17651	23754	155	F053A	27.33 ± 2.76	21.22 ± 0.49	9.90	1.29	0.29	<1.67E-06	2.18	N	1,2
18280	⋯	156	K124A	4.21 ± 1.87	2.64 ± 0.07	2.25	<3.71	<2.71	<2.78E-05	0.84	N	1,2
19884	27274	167	K067A	2.92 ± 0.84	4.72 ± 0.07	3.48	0.62	−0.38	<1.17E-06	−2.14	N	1,2
22263	30495	177	G029A	86.02 ± 5.19	10.43 ± 0.18	16.58	8.25	7.25	3.10E-05	14.56	Y	1,2,5
22449	30652	178	F003A	61.78 ± 4.34	58.96 ± 1.04	14.24	1.05	0.05	<6.93E-07	0.63	N	1,2
23311	32147	183	K024A	9.90 ± 2.12	13.18 ± 0.21	4.68	0.75	−0.25	<1.56E-06	−1.54	N	1,2
23693	33262	189	F012A	32.91 ± 3.11	17.19 ± 0.31	10.57	1.91	0.91	1.19E-05	5.03	Y	1,2,5

Table 3
(Continued)

HIP	HD	GJ	UNS	F_{obs}^{100a} (mJy)	F_{star}^{100b} (mJy)	$F_{obs}^{100}/\sigma_{obs}^{100c}$	$F_{obs}^{100}/F_{star}^{100d}$	$F_{dust}^{100}/F_{star}^{100d}$	L_{dust}/L_{star}^{e}	SNR_{dust} [f]	Dust Detec.?	Set[g]
25544	36435	204.1	G095A	3.16 ± 2.39	3.32 ± 0.05	1.32	<3.12	<2.12	<9.30E-06	−0.07	N	1,2
26394	39091	9189	G085A	16.06 ± 2.43	7.95 ± 0.15	6.60	2.02	1.02	1.51E-06	3.33	Y	1,3a,5,6
27072	38393	216A	F006A	44.44 ± 5.22	43.79 ± 0.81	8.51	1.01	0.01	<1.04E-06	0.12	N	1,2
	38392	216B	F006B	11.53 ± 2.76	11.91 ± 0.18	4.18	0.97	−0.03	<4.04E-06	−0.14	N	1,2
27188	⋯	215	K082A	4.91 ± 2.30	3.12 ± 0.07	2.14	<3.79	<2.79	<3.08E-05	0.78	N	1,2
27887	40307	⋯	K065A	8.40 ± 1.17	5.08 ± 0.06	7.20	1.66	0.66	<8.51E-06	2.85	N	1,4,7
28103	40136	225	F028	45.18 ± 3.22	27.56 ± 0.50	14.04	1.64	0.64	1.10E-05	5.41	Y	1,2,5
28442	40887	225.2	⋯	-0.74 ± 0.70	5.14 ± 0.13	−1.06	<0.41	<-0.59	<-5.23E-06	−8.26	N	1,2
29568	43162	3389	G056A	6.57 ± 1.13	5.50 ± 0.14	5.81	1.20	0.20	<3.37E-06	0.94	N	1,2
32439	46588	240.1	F056A	8.49 ± 1.57	8.58 ± 0.15	5.40	0.99	−0.01	<1.60E-06	−0.06	N	1,2
32480	48682	245	F044A	263.67 ± 20.20	11.16 ± 0.45	13.05	23.62	22.62	6.24E-05	12.49	Y	1,2,5
33277	50692	252	G065A	6.66 ± 1.29	7.75 ± 0.14	5.15	0.86	−0.14	<1.25E-06	−0.84	N	1,2
34017	52711	262	G093A	7.30 ± 1.25	6.56 ± 0.19	5.85	1.11	0.11	<2.39E-06	0.59	N	1,2
34052	53680	264	G059C	−0.01 ± 2.90	2.42 ± 0.05	0.00	<3.60	<2.60	<2.33E-05	−0.84	N	1,2
34065	53705	264.1A	G059A	8.42 ± 2.65	10.01 ± 0.26	3.18	0.84	−0.16	<2.31E-06	−0.60	N	1,2
34069	53706	264.1B	G059B	1.22 ± 1.92	4.28 ± 0.09	0.64	<1.63	<0.63	<3.03E-06	−1.59	N	1,2
35136	55575	1095	F045A	11.36 ± 1.60	9.45 ± 0.19	7.12	1.20	0.20	<2.45E-06	1.19	N	1,2
37288	⋯	281	K099A	3.77 ± 2.04	2.01 ± 0.10	1.85	<4.93	<3.93	<4.23E-05	0.86	N	1,2
37349	61606	282A	K090A	−3.24 ± 1.76	4.83 ± 0.09	−1.85	<1.09	<0.09	<5.64E-07	−4.59	N	1,2
	⋯	282B	K090B	0.68 ± 2.83	2.93 ± 0.09	0.24	<3.12	<2.12	<2.25E-05	−0.80	N	1,2
38784	62613	290	G062A	3.09 ± 0.97	4.57 ± 0.08	3.17	0.68	−0.32	<1.30E-06	−1.51	N	1,2
40693	69830	302	G022A	10.25 ± 1.17	9.04 ± 0.23	8.76	1.13	0.13	<2.37E-06[h]	1.02	N	1,4,7
40702	71243	305	F077A	27.65 ± 2.76	24.23 ± 0.43	10.02	1.14	0.14	<1.16E-06	1.22	N	1,2
40843	69897	303	F061A	11.79 ± 2.35	11.10 ± 0.52	5.01	1.06	0.06	<1.99E-06	0.29	N	1,2, (conf.?)
42438	72905	311	G036A	20.72 ± 1.51	8.90 ± 0.18	13.73	2.33	1.33	7.73E-06	7.78	Y	1,2,5
42748	⋯	319A&B	K121AB	4.40 ± 1.89	2.61 ± 0.07	2.32	<3.86	<2.86	<3.80E-05	0.94	N	1,2
43587	75732	324A	K060A	8.39 ± 1.66	9.95 ± 0.25	5.04	0.84	−0.16	<1.68E-06	−0.93	N	1,3a,7
	⋯	324B	K060B	−5.21 ± 2.63	0.86 ± 0.05	−1.98	<9.18	<8.18	<2.29E-04	−2.31	N	1,2
43726	76151	327	G068A	15.25 ± 1.50	6.48 ± 0.11	10.15	2.35	1.35	1.58E-05	5.82	Y	1,2,5
44248	76943	332A&B	F040AB	31.07 ± 2.35	27.95 ± 0.58	13.22	1.11	0.11	<9.26E-07	1.29	N	1,2
44722	⋯	334	K097A	3.00 ± 1.54	2.67 ± 0.08	1.95	<2.86	<1.86	<2.32E-05	0.22	N	1,2
44897	78366	334.2	G094A	6.61 ± 0.95	6.06 ± 0.10	6.95	1.09	0.09	<1.86E-06	0.58	N	1,2
45343	79210	338A	K011A	9.52 ± 1.96	10.78 ± 0.51	4.85	0.88	−0.12	<4.96E-06	−0.62	N	1,2
120005	79211	338B	K011B	9.58 ± 1.96	12.64 ± 0.45	4.88	0.76	−0.24	<2.77E-06	−1.52	N	1,2
46580	82106	349	K064A	7.19 ± 1.06	5.24 ± 0.09	6.78	1.37	0.37	<6.44E-06	1.83	N	1,2
47592	84117	364	F031A	7.37 ± 1.77	13.98 ± 0.27	4.17	0.53	−0.47	<−2.81E-07	−3.70	N	1,2
48113	84737	368	G086A	8.53 ± 1.68	13.77 ± 0.25	5.08	0.62	−0.38	<−4.88E-08	−3.08	N	1,2
49081	86728	376	G040A	7.96 ± 1.71	11.63 ± 0.24	4.66	0.68	−0.32	<4.59E-07	−2.13	N	1,2
49908	88230	380	K005A	22.57 ± 1.55	25.27 ± 0.54	14.58	0.89	−0.11	<8.05E-07	−1.65	N	1,2
53721	95128	407	G033A	12.11 ± 2.15	15.00 ± 0.28	5.63	0.81	−0.19	<8.27E-07	−1.33	N	1,3a,7
54646	97101	414A	K056A	5.77 ± 1.06	4.25 ± 0.99	5.44	1.36	0.36	<8.89E-06	1.04	N	1,2
	⋯	414B	K056B	0.46 ± 1.01	3.40 ± 0.18	0.45	<1.03	<0.03	<4.34E-07	−2.87	N	1,2
55846	99491	429A	G079A	5.21 ± 2.03	5.43 ± 0.19	2.57	<2.08	<1.08	<4.84E-06	−0.11	N	1,2
55848	99492	429B	G079B	2.66 ± 1.85	3.22 ± 0.06	1.44	<2.55	<1.55	<9.22E-06	−0.30	N	1,3a,6
56452	100623	432A	K029A	13.58 ± 1.75	10.38 ± 0.18	7.77	1.31	0.31	<4.06E-06	1.82	N	1,2
	⋯	432B	K029B	0.99 ± 1.57	0.00 ± 0.00	0.63	<13843.	<13842.49	<1.17E-02	0.63	N	1,2
56997	101501	434	G013A	14.01 ± 2.33	14.75 ± 0.28	6.02	0.95	−0.05	<1.78E-06	−0.31	N	1,2

Table 3
(Continued)

HIP	HD	GJ	UNS	F_{obs}^{100a} (mJy)	F_{star}^{100b} (mJy)	$F_{obs}^{100}/\sigma_{obs}^{100c}$	$F_{obs}^{100}/F_{star}^{100d}$	$F_{dust}^{100}/F_{star}^{100d}$	L_{dust}/L_{star}^{e}	SNR_{dust} [f]	Dust Detec.?	Set[g]
56998	101581	435	K059A	2.61 ± 1.95	4.04 ± 0.10	1.34	<2.09	<1.09	<8.28E-06	−0.74	N	1,2
57443	102365	442A	G012A	18.73 ± 2.30	20.35 ± 0.35	8.14	0.92	−0.08	<1.03E-06	−0.69	N	1,4,6
	⋯	442B	G012B	−1.10 ± 1.94	0.69 ± 0.02	−0.57	<8.45	<7.45	<2.69E-04	−0.92	N	1,2
57507	102438	446	G069A	4.79 ± 1.14	4.86 ± 0.08	4.20	0.98	−0.02	<2.80E-06	−0.07	N	1,2
57757	102870	449	F009A	59.37 ± 4.16	49.01 ± 0.96	14.29	1.21	0.21	<1.46E-06	2.43	N	1,2
57939	103095	451A	K028A	6.40 ± 1.18	7.45 ± 0.14	5.42	0.86	−0.14	<1.75E-06	−0.88	N	1,2
58345	103932	453	K034A	7.65 ± 0.99	8.13 ± 0.17	7.73	0.94	−0.06	<2.31E-06	−0.48	N	1,2
59199	105452	455.3	F030A	27.61 ± 2.87	21.63 ± 0.40	9.62	1.28	0.28	<1.39E-06	2.06	N	1,2
61094	⋯	471	K081A	2.87 ± 1.79	2.26 ± 0.13	1.60	<3.64	<2.64	<3.23E-05	0.34	N	1,2
61174	109085	471.2	F063A	254.27 ± 16.14	16.99 ± 1.39	15.75	14.97	13.97	1.78E-04	14.64	Y	1,2,5
61317	109358	475	G007AB	28.74 ± 2.52	31.44 ± 0.57	11.42	0.91	−0.09	<5.34E-07	−1.05	N	1,2
61901	110315	481	K092A	3.49 ± 2.32	4.06 ± 0.06	1.50	<2.58	<1.58	<1.29E-05	−0.24	N	1,2
62207	110897	484	F050A	59.28 ± 3.98	6.58 ± 0.14	14.88	9.01	8.01	2.37E-05	13.22	Y	1,2,5
62523	111395	486.1	G057A	4.51 ± 1.01	5.58 ± 0.10	4.45	0.81	−0.19	<1.42E-06	−1.04	N	1,2
62687	111631	488	K036A	9.55 ± 2.38	4.96 ± 0.06	4.02	1.92	0.92	<2.50E-05	1.93	N	1,2
64394	114710	502	G010A	22.16 ± 2.08	28.41 ± 0.53	10.66	0.78	−0.22	<−1.45E-09	−2.91	N	1,2
64792	115383	504	G073A	13.15 ± 1.24	12.03 ± 0.25	10.63	1.09	0.09	<1.31E-06	0.89	N	1,3a,6
64924	115617	506	G008A	152.48 ± 10.03	24.48 ± 0.47	15.20	6.23	5.23	2.85E-05	12.75	Y	1,4,5,7
65026	115953	508	⋯	9.30 ± 1.00	9.38 ± 0.26	9.31	0.99	−0.01	<4.21E-06	−0.08	N	1,2
65352	116442	3781A	G050A	4.21 ± 2.19	3.80 ± 0.06	1.92	<2.84	<1.84	<9.15E-06	0.19	N	1,2
65355	116443	3782B	G050B	5.34 ± 2.20	3.48 ± 0.06	2.43	<3.44	<2.44	<1.37E-05	0.85	N	1,2
65721	117176	512.1	⋯	41.04 ± 2.55	20.77 ± 0.42	16.10	1.98	0.98	1.00E-05	7.85	Y	1,3a,5,6
66459	⋯	519	K041A	1.26 ± 1.63	3.33 ± 0.08	0.77	<1.85	<0.85	<9.60E-06	−1.27	N	1,2
66675	118926	521.1	K109A	6.03 ± 2.90	2.09 ± 0.06	2.08	<7.04	<6.04	<7.42E-05	1.36	N	1,2
67090	⋯	525	K070A	2.60 ± 1.96	1.88 ± 0.07	1.32	<4.51	<3.51	<4.40E-05	0.36	N	1,2
67275	120136	527A	F036A	19.20 ± 3.69	14.47 ± 66.26	5.20	1.33	0.33	<2.48E-06	0.07	N	1,3b,6
67275	⋯	527B	F036B	−4.80 ± 4.19	1.28 ± 0.03	−1.14	<9.81	<8.81	<1.37E-04	−1.45	N	1,2
67308	120036	1177A	K103A	3.90 ± 1.80	3.04 ± 0.13	2.16	<3.06	<2.06	<2.12E-05	0.47	N	1,2
67308	⋯	1177B	K103B	−1.15 ± 1.79	2.72 ± 0.16	−0.64	<1.97	<0.97	<1.00E-05	−2.15	N	1,2
67487	120467	529	K095A	4.25 ± 2.49	4.07 ± 0.07	1.71	<2.87	<1.87	<1.70E-05	0.07	N	1,2
67691	234078	532	K091A	1.14 ± 2.29	2.99 ± 0.11	0.50	<2.68	<1.68	<1.66E-05	−0.81	N	1,2
68184	122064	⋯	K032A	8.61 ± 1.03	9.60 ± 0.18	8.32	0.90	−0.10	<1.41E-06	−0.95	N	1,2
70218	⋯	546	K096A	2.88 ± 1.59	3.23 ± 0.05	1.82	<2.37	<1.37	<1.31E-05	−0.21	N	1,2
70319	126053	547	G063A	3.29 ± 0.87	5.47 ± 0.08	3.78	0.60	−0.40	<2.97E-07	−2.50	N	1,2
70497	126660	549A	F026A	33.29 ± 3.06	29.67 ± 0.57	10.90	1.12	0.12	<1.23E-06	1.17	N	1,2
	⋯	549B	F026B	1.23 ± 2.87	1.07 ± 0.06	0.43	<9.18	<8.18	<1.42E-04	0.06	N	1,2
71181	128165	556	K072A	10.53 ± 1.03	5.17 ± 0.07	10.19	2.03	1.03	8.16E-06	5.17	Y	1,2,5
71284	128167	557	F039A	35.52 ± 2.93	16.50 ± 0.31	12.11	2.15	1.15	1.13E-05	6.44	Y	1,2,5
71908	128898	560A	A010A	39.53 ± 4.53	35.84 ± 0.78	8.72	1.10	0.10	<7.80E-07	0.80	N	1,2
	128898	560B	A010B	0.11 ± 3.94	2.70 ± 0.08	0.03	<4.41	<3.41	⋯	−0.66	N	1,2
71957	129502	9491	F062A	35.41 ± 2.65	28.01 ± 1.08	13.37	1.26	0.26	<1.28E-06	2.59	N	1,2
73182	131976	570B	K008B	16.86 ± 2.06	18.10 ± 0.51	8.19	0.93	−0.07	<4.30E-06	−0.58	N	1,2
73184	131977	570A	K008A	22.06 ± 2.21	23.45 ± 0.43	9.98	0.94	−0.06	<1.64E-06	−0.62	N	1,2
73996	134083	578	F076A	7.36 ± 1.53	11.08 ± 0.21	4.81	0.66	−0.34	<1.95E-07	−2.40	N	1,2
75277	136923	⋯	G101A	5.02 ± 2.11	3.14 ± 0.05	2.37	<3.62	<2.62	<1.22E-05	0.89	N	1,2
76779	139763	⋯	K126A	3.99 ± 2.17	2.57 ± 0.06	1.84	<4.08	<3.08	<3.07E-05	0.65	N	1,2
77257	141004	598	G019A	27.85 ± 2.22	25.50 ± 0.48	12.54	1.09	0.09	<1.20E-06	1.03	N	1,2

Table 3
(Continued)

HIP	HD	GJ	UNS	F_{obs}^{100a} (mJy)	F_{star}^{100b} (mJy)	$F_{obs}^{100}/\sigma_{obs}^{100c}$	$F_{obs}^{100}/F_{star}^{100d}$	$F_{dust}^{100}/F_{star}^{100d}$	L_{dust}/L_{star}^{e}	SNR_{dust} [f]	Dust Detec.?	Set[g]
77760	142373	602	G052A	19.76 ± 2.20	23.12 ± 0.41	9.00	0.85	−0.15	<4.92E-07	−1.50	N	1,2
78072	142860	603	F011A	33.54 ± 2.82	35.05 ± 0.64	11.89	0.96	−0.04	<5.49E-07	−0.52	N	1,2
78459	143761	606.2	G064A	7.50 ± 1.87	11.16 ± 0.20	4.02	0.67	−0.33	<6.25E-07	−1.95	N	1,3a,6
78775	144579	611A	K098A	3.29 ± 1.17	5.18 ± 0.07	2.82	<1.31	<0.31	<1.49E-06	−1.61	N	1,2
	⋯	611B	K098B	-1.09 ± 1.40	0.16 ± 0.00	−0.78	<25.81	<24.81	<4.62E-04	−0.89	N	1,2
79248	145675	614	⋯	3.79 ± 0.76	5.30 ± 0.07	5.01	0.72	−0.28	<6.79E-07	−1.99	N	1,3a,6
79755	147379	617A	K039A	0.24 ± 3.51	4.74 ± 0.05	0.07	<2.27	<1.27	<1.34E-05	−1.28	N	1,2
79762	⋯	617B	K039B	6.25 ± 3.81	2.76 ± 0.11	1.64	<6.39	<5.39	<1.03E-04	0.92	N	1,2
80725	148653	⋯	⋯	2.78 ± 0.81	4.68 ± 0.11	3.43	0.59	−0.41	<6.48E-07	−2.31	N	1,2
82003	151288	638	K031A	4.43 ± 1.80	5.72 ± 0.32	2.46	<1.72	<0.72	<5.99E-06	−0.70	N	1,2
83389	154345	651	G088A	3.80 ± 0.84	4.07 ± 0.06	4.53	0.93	−0.07	<2.41E-06	−0.32	N	1,3a,6
83990	154577	656	K080A	11.45 ± 3.29	3.83 ± 0.06	3.48	2.99	1.99	<2.75E-05	2.32	N	1,2
84862	157214	672	G035A	12.21 ± 1.37	12.15 ± 0.21	8.88	1.00	0.00	<1.29E-06	0.04	N	1,2
85235	158633	675	K062A	34.66 ± 3.03	6.29 ± 0.09	11.46	5.51	4.51	3.05E-05	9.37	Y	1,2,5
85295	157881	673	K021A	10.01 ± 1.98	9.99 ± 0.45	5.04	1.00	0.00	<5.78E-06	0.01	N	1,2
86796	160691	691	G047	14.35 ± 2.40	15.07 ± 0.30	5.99	0.95	−0.05	<1.60E-06	−0.30	N	1,3a,7
88601	165341	702A	K007A	35.76 ± 3.75	37.59 ± 0.89	9.54	0.95	−0.05	<1.20E-06	−0.48	N	1,2
88601	165341	702A	K007B	29.53 ± 3.46	27.82 ± 4.88	8.53	1.06	0.06	<2.09E-06	0.29	N	1,2
88972	166620	706	K044A	7.46 ± 1.22	8.35 ± 0.13	6.09	0.89	−0.11	<1.87E-06	−0.72	N	1,2
89042	165499	705.1	G075A	11.06 ± 1.38	9.81 ± 0.18	8.02	1.13	0.13	<1.88E-06	0.90	N	1,2
89211	166348	707	K068A	11.30 ± 2.79	3.76 ± 0.06	4.05	3.00	2.00	<4.02E-05	2.70	N	1,2
91009	234677	719	⋯	6.87 ± 0.87	5.47 ± 0.08	7.93	1.25	0.25	<7.06E-06	1.60	N	1,2
92043	173667	725.2	F073	26.53 ± 2.53	23.91 ± 0.44	10.50	1.11	0.11	<1.16E-06	1.02	N	1,2
95149	181321	755	G091A	4.67 ± 2.60	4.30 ± 0.06	1.80	<2.90	<1.90	<7.04E-06	0.14	N	1,2
95995	184467	762.1	⋯	3.64 ± 0.78	6.40 ± 0.10	4.64	0.57	−0.43	<−3.60E-07	−3.49	N	1,2
96100	185144	764	G003	32.10 ± 2.66	31.55 ± 0.52	12.08	1.02	0.02	<1.32E-06	0.20	N	1,2
97944	188088	770	⋯	9.86 ± 1.05	11.23 ± 0.42	9.37	0.88	−0.12	<1.11E-06	−1.21	N	1,2
98698	190007	775	K063A	4.99 ± 1.89	5.39 ± 0.07	2.63	<1.98	<0.98	<7.46E-06	−0.21	N	1,2
98959	189567	776	G077A	4.64 ± 0.90	6.38 ± 0.12	5.15	0.73	−0.27	<5.68E-07	−1.92	N	1,2, (4?,6?)
99240	190248	780	⋯	69.14 ± 2.28	70.31 ± 3.59	30.28	0.98	−0.02	<3.32E-07	−0.28	N	1,2
99701	191849	784	K012A	19.42 ± 2.95	10.63 ± 0.43	6.59	1.83	0.83	<2.03E-05	2.95	N	1,2
99825	192310	785	K027A	10.99 ± 1.98	14.45 ± 0.54	5.56	0.76	−0.24	<9.31E-07	−1.69	N	1,4,7
100925	194640	790	G098A	4.87 ± 2.37	4.36 ± 0.06	2.05	<2.75	<1.75	<7.27E-06	0.21	N	1,2
101955	196795	795	⋯	4.12 ± 1.00	6.20 ± 0.14	4.10	0.66	−0.34	<1.46E-06	−2.06	N	1,2
101997	196761	796	G037A	4.75 ± 1.10	5.93 ± 0.10	4.34	0.80	−0.20	<1.55E-06	−1.07	N	1,2
102186	196877	798	K057A	−2.81 ± 1.80	3.01 ± 0.13	−1.56	<1.79	<0.79	<7.88E-06	−3.22	N	1,2
102485	197692	805	F027A	25.15 ± 2.90	23.18 ± 0.43	8.67	1.08	0.08	<1.14E-06	0.67	N	1,2
104092	200779	818	K116A	2.73 ± 2.24	3.55 ± 0.06	1.22	<2.67	<1.67	<1.49E-05	−0.36	N	1,2
104214	201091	820A	K002A	47.22 ± 3.80	51.64 ± 1.28	12.42	0.91	−0.09	<1.14E-06	−1.10	N	1,2
104217	201092	820B	K002B	35.78 ± 3.37	43.53 ± 0.99	10.61	0.82	−0.18	<6.09E-07	−2.20	N	1,2
104440	⋯	818.1 C	F079C	−0.19 ± 2.55	0.22 ± 0.00	−0.07	<35.24	<34.24	<6.39E-04	−0.16	N	1,2
105090	202560	825	K004A	31.44 ± 2.92	31.23 ± 0.55	10.75	1.01	0.01	<3.44E-06	0.07	N	1,2
105858	203608	827	F007A	31.43 ± 2.66	27.68 ± 0.50	11.82	1.14	0.14	<1.27E-06	1.39	N	1,2
106696	205390	833	K101A	4.75 ± 1.17	4.40 ± 0.07	4.06	1.08	0.08	<5.02E-06	0.31	N	1,2
107350	206860	836.7	G080A	16.38 ± 1.31	6.14 ± 0.12	12.48	2.67	1.67	9.43E-06	7.77	Y	1,2,5
107649	207129	838	G053A	343.95 ± 19.86	8.82 ± 0.19	17.32	38.99	37.99	9.85E-05	16.88	Y	1,2,5
108870	209100	845	K003A	57.59 ± 3.43	59.08 ± 1.19	16.78	0.97	−0.03	<1.05E-06	−0.41	N	1,2

Table 3
(Continued)

HIP	HD	GJ	UNS	F_{obs}^{100} [a] (mJy)	F_{star}^{100} [b] (mJy)	$F_{obs}^{100}/\sigma_{obs}^{100}$ [c]	$F_{obs}^{100}/F_{star}^{100}$ [d]	$F_{dust}^{100}/F_{star}^{100}$ [d]	L_{dust}/L_{star} [e]	SNR_{dust} [f]	Dust Detec.?	Set [g]
109422	210302	849.1	F064A	11.37 ± 2.08	11.97 ± 0.33	5.46	0.95	−0.05	<1.26E-06	−0.29	N	1,2
110443	211970	1267	K076A	4.04 ± 1.97	2.82 ± 0.06	2.05	<3.52	<2.52	<2.78E-05	0.62	N	1,2
111960	214749	868	K077A	−1.77 ± 1.89	4.20 ± 0.08	−0.94	<1.35	<0.35	<2.82E-06	−3.15	N	1,2
112447	215648	872A	F043A	25.45 ± 2.83	28.50 ± 0.57	8.98	0.89	−0.11	<5.82E-07	−1.05	N	1,2
	⋯	872B	F043B	−1.46 ± 2.45	1.06 ± 0.02	−0.60	<6.92	<5.92	<1.10E-04	−1.03	N	1,2
112774	216133	875	K088A	2.63 ± 1.99	1.96 ± 0.10	1.32	<4.39	<3.39	<4.24E-05	0.34	N	1,2
113283	216803	879	K019A	11.13 ± 2.17	12.55 ± 0.21	5.12	0.89	−0.11	<3.04E-06	−0.65	N	1,2
113421	217107	⋯	G102AB	2.79 ± 1.85	6.20 ± 0.11	1.50	<1.35	<0.35	<1.39E-06	−1.84	N	1,3a,7
113576	217357	884	K022A	9.71 ± 1.19	7.87 ± 0.13	8.15	1.23	0.23	<7.26E-06	1.53	N	1,2
114361	218511	1279	K114A	16.59 ± 2.58	3.11 ± 0.18	6.43	5.34	4.34	3.71E-05	5.21	Y	1,2,5
116215	221503	898	K112A	2.48 ± 2.13	3.11 ± 0.05	1.16	<2.86	<1.86	<1.78E-05	−0.30	N	1,2
116745	222237	902	K052A	4.96 ± 1.07	6.16 ± 0.09	4.62	0.81	−0.19	<2.22E-06	−1.11	N	1,2
116763	222335	902.1	G087A	2.87 ± 2.02	3.22 ± 0.06	1.42	<2.77	<1.77	<8.64E-06	−0.17	N	1,2
116771	222368	904	F021A	43.60 ± 3.29	29.41 ± 0.64	13.25	1.48	0.48	8.21E-07	4.24	Y	1,2,5
120005	79211	338B	K011B	9.58 ± 1.96	12.64 ± 0.45	4.88	0.76	−0.24	<2.77E-06	−1.52	N	1,2
	26976	166B&C	K006BC	1.01 ± 1.86	3.31 ± 0.17	0.54	<1.99	<0.99	<1.99E-05	−1.24	N	1,2

Notes.

[a] Observed PACS flux at 100 μm with 1σ uncertainty (σ_{obs}^{100}).

[b] Estimated photospheric prediction at 100 μm with 1σ uncertainty (σ_{star}^{100}).

[c] Stars with significant detected emission have $F_{obs}^{100}/\sigma_{obs}^{100} > 3$.

[d] Observed flux ratio ($F_{obs}^{100}/F_{star}^{100}$) and dust excess flux ratio ($F_{dust}^{100}/F_{star}^{100}$, where $F_{dust} = F_{obs}^{100} - F_{star}^{100}$). In both cases, the 3σ upper limits (preceded by "<" symbol) are given for stars without significant detected emission and are calculated assuming the observed flux is $F_{obs}^{100} + 3\sigma_{obs}^{100}$, for stars with $0 < F_{obs}^{100}/\sigma_{obs}^{100} < 3$, and $3\sigma_{obs}^{100}$, for stars with $F_{obs}^{100}/\sigma_{obs}^{100} < 0$.

[e] Fractional luminosity of the dust excess emission. For stars with excess detections ($SNR_{dust} > 3$), the fractional luminosity is calculated following Kennedy et al. (2012a, 2012b). For stars with excess nondetections ($SNR_{dust} < 3$), the 3σ upper limit to the fractional luminosity is calculated from $\frac{L_{dust}}{L_{star}} = \left(\frac{T_{dust}}{T_{star}}\right)^4 \left(\frac{e^{x_{dust}} - 1}{e^{x_{star}} - 1}\right) F_{obs}^{100} - F_{star}^{100} \cdot F_{star}^{100}$ following Equation (4) in Beichman et al. (2006) and assuming the observed flux is $F_{obs}^{100} + 3\sigma_{obs}^{100}$, for stars with $F_{obs}^{100}/\sigma_{obs}^{100} > 0$, and $3\sigma_{obs}^{100}$, for stars with $F_{obs}^{100}/\sigma_{obs}^{100} < 0$. In this expression, $x = \frac{h\nu}{kT}$, where ν is the frequency corresponding to 100 μm, $T_{star} = T_{eff}$ is the effective stellar photospheric temperature, and T_{dust} is assumed to be 50 K (as in Eiroa et al. 2013).

[f] Signal-to-noise ratio of the excess emission, given by $SNR_{dust} = \frac{F_{obs}^{100} - F_{star}^{100}}{\sqrt{\sigma_{obs}^{100^2} + \sigma_{star}^{100^2}}}$.

[g] For label information, see Table 1. Systems that may be subject to confusion are labeled as "(conf.?)." The "set" classifications of the systems with unconfirmed planetary systems—namely, HIP 16537 ($= \epsilon$ Eri), HIP 8102 ($= \tau$ Cet), and HIP 98959—are indicated in parentheses.

[h] Note that this upper limit is based on the nondetection at 100 μm; this star, however, has an excess emission at 8–35 μm with an inferred fractional luminosity of $L_{dust}/L_{star} = 2{\cdot}10^{-4}$ (Lisse et al. 2007).

Table 4
Planetary System Properties[a]

HIP	HD	GJ	UNS	Planet Name	$M_{pl}\sin(i)$ (M_{Jup})	a (AU)	e	R_{dust} (AU)	Set	Ref.[b]
3093	3651	27	K045A	b	0.229	0.29	0.60	⋯	3a,6	(1)
7513	9826	61	F020A	b	0.669	0.06	0.01	⋯	3a,7	(2)
7513	9826	61	F020A	c	1.919	0.83	0.22	⋯	3a,7	(2)
7513	9826	61	F020A	d	4.116	2.52	0.27	⋯	3a,7	(2)
7978	10647	3109	F051A	b	0.925	2.02	0.16	40.3 ± 5.9	3a,6	(3)
12653	17051	108	F046A	b	2.047	0.92	0.14	⋯	3a,6	(3)
15510	20794	139	G005A	b	0.008	0.12	0.00	16.5 ± 7.5	4,7	(4)
15510	20794	139	G005A	c	0.007	0.20	0.00	16.5 ± 7.5	4,7	(4)
15510	20794	139	G005A	d	0.015	0.35	0.00	16.5 ± 7.5	4,7	(4)
26394	39091	9189	G085A	b	10.088	3.35	0.64	51.3 ± 30.2	3a,6	(3)
27887	40307	⋯	K065A	c	0.021	0.08	0.00	⋯	4,7	(5)
27887	40307	⋯	K065A	d	0.028	0.13	0.00	⋯	4,7	(5)
27887	40307	⋯	K065A	b	0.013	0.05	0.00	⋯	4,7	(5)
40693	69830	302	G022A	c	0.037	0.19	0.13	⋯	4,7	(6)
40693	69830	302	G022A	d	0.056	0.63	0.07	⋯	4,7	(6)
40693	69830	302	G022A	b	0.032	0.08	0.10	⋯	4,7	(6)
43587	75732	324A	K060A	e	0.026	0.02	0.00	⋯	3a,7	(7)
43587	75732	324A	K060A	f	0.173	0.77	0.32	⋯	3a,7	(7)
43587	75732	324A	K060A	b	0.801	0.11	0.00	⋯	3a,7	(7)
43587	75732	324A	K060A	d	3.545	5.47	0.02	⋯	3a,7	(7)
43587	75732	324A	K060A	c	0.165	0.24	0.07	⋯	3a,7	(7)
53721	95128	407	G033A	c	0.546	3.57	0.10	⋯	3a,7	(8)
53721	95128	407	G033A	b	2.546	2.10	0.03	⋯	3a,7	(8)
55848	99492	429B	G079B	b	0.106	0.12	0.25	⋯	3a,6	(3)
57443	102365	442A	G012A	b	0.051	0.46	0.34	⋯	4,6	(9)
64924	115617	506	G008A	b	0.016	0.05	0.12	15.9 ± 1.5	4,7	(10)
64924	115617	506	G008A	c	0.033	0.22	0.14	15.9 ± 1.5	4,7	(10)
64924	115617	506	G008A	d	0.072	0.47	0.35	15.9 ± 1.5	4,7	(10)
65721	117176	512.1		b	7.461	0.48	0.40	14.0	3a,6	(3)
67275	120136	527A	F036A	b	4.130	0.05	0.02	⋯	3b,6	(11)
78459	143761	606.2	G064A	b	1.064	0.23	0.06	⋯	3a,6	(3)
79248	145675	614		b	5.215	2.93	0.37	⋯	3a,6	(12)
83389	154345	651	G088A	b	0.957	4.21	0.04	⋯	3a,6	(13)
86796	160691	691	G047	b	1.746	1.53	0.13	⋯	3a,7	(14)
86796	160691	691	G047	e	0.543	0.94	0.07	⋯	3a,7	(14)
86796	160691	691	G047	c	1.889	5.34	0.10	⋯	3a,7	(14)
86796	160691	691	G047	d	0.035	0.09	0.17	⋯	3a,7	(14)
99825	192310	785	K027A	c	0.074	1.18	0.32	⋯	4,7	(4)
99825	192310	785	K027A	b	0.053	0.32	0.13	⋯	4,7	(4)
113421	217107	⋯	G102AB	c	2.615	5.33	0.52	⋯	3a,7	(2)
113421	217107	⋯	G102AB	b	1.401	0.08	0.13	⋯	3a,7	(2)
				Unconfirmed Planetary Systems[c]						
16537	22049	144	K001A	b	1.054	3.38	0.25	36.0	3a,6	(15)
8102	10700	71	G002A	b	0.0063	0.105	0.16	8.5	4,7	(16)
8102	10700	71	G002A	c	0.0097	0.195	0.03	8.5	4,7	(16)
8102	10700	71	G002A	d	0.011	0.374	0.08	8.5	4,7	(16)
8102	10700	71	G002A	e	0.013	0.552	0.05	8.5	4,7	(16)
8102	10700	71	G002A	f	0.02	1.35	0.03	8.5	4,7	(16)
98959	189567	776	G077A	b	0.0316	0.11	0.23	⋯	3a,6	(17)

Notes.
[a] Planetary system properties from http://exoplanets.org.
[b] Orbit references are (1) Wittenmyer et al. (2009), (2) Wright et al. (2009), (3) Butler et al. (2006), (4) Pepe et al. (2011), (5) Mayor et al. (2009), (6) Lovis et al. (2006), (7) Endl et al. (2012), (8) Gregory et al. (2010), (9) Tinney et al. (2011), (10) Vogt et al. (2010), (11) Brogi et al. (2012), (12) Wittenmyer et al. (2007), (13) Wright et al. (2008), (14) Pepe et al. (2007), (15) Hatzes et al. (2000), (16) Tuomi et al. (2013), and (17) Mayor et al. (2011).
[c] Unconfirmed planetary systems are HD 22049 (ϵ Eri), HD 10700 (τ Cet), and HD 189567.

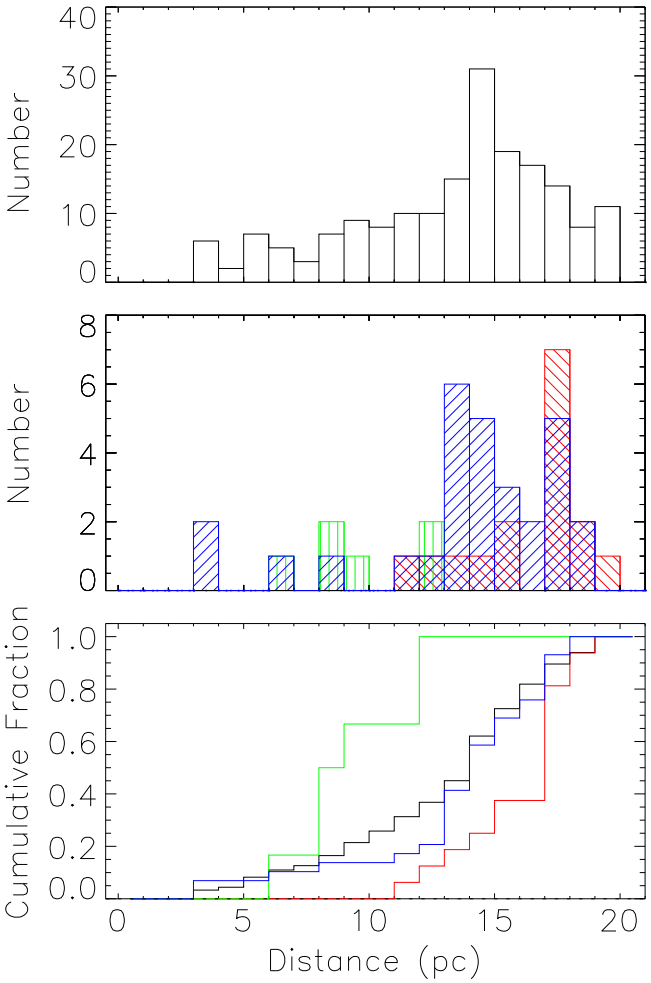

Figure 1. Distribution of distances. Top: stars without known planets (Set 2). Middle: the line-filled colored histograms correspond to the high-mass planet sample (Set 3; in red, with hatching from the top left to the bottom right), low-mass planet sample (Set 4; in green, with vertical hatching), and debris disk sample (Set 5; in blue, with hatching from the top right to the bottom left). Bottom: cumulative fraction of distances (same color code as above).

emission is a good tracer of the cold KB-like dust, and we will use it as our reference wavelength. The analysis presented in this paper is limited to cold KB-like debris disks (where cold refers to debris disks detected at 70–100 μm); we are not including the warm debris disks identified by *Spitzer* at 24 μm and with no excess at 70 μm (under this category there is only one planet-bearing star, HD 69830).

Note that there are several targets harboring debris disks and/or planets that were observed with *Spitzer* but were not observed by the *Herschel* DEBRIS and DUNES surveys because of their high level of background emission.

2.6. Sets 6 and 7: Single-/Multiple-planet Sample

Set 6 is the subset of stars from Set 1 known as of August 2014 to harbor single-planet systems, whereas Set 7 is the subset of stars with multiple known planets.

2.7. Sets 1y–5y and 1o–5o: Young/Old Samples

If debris disks evolve with time, and the samples compared have different age distributions, this will introduce a bias in our analysis. We therefore divide the samples into stars younger than 1 Gyr (labeled as Sets 1y–5y) and stars older than 1 Gyr (Sets 1o–5o; our sample has no hot Jupiters in Set 3o), limiting the comparison to sets of similar ages (i.e., within the o or y groups). We find that the distribution of ages in the samples considered (Figure 2) show that planet-bearing stars (Sets 3 and 4) tend to be older on average than the stars in the no-planet sample (Set 2); this is because Gyr-old stars have low magnetic activity, implying lower levels of radial velocity jitter that facilitate the Doppler studies. While this might result in planet-bearing stars having fewer debris detections if debris levels decrease with age, Figure 2 shows little evidence for evolution in disk detectability with time, and this is discussed further in Section 3.1.

2.8. Sets 1h and 1l: High-/Low-metallicity Samples

To explore the role of stellar metallicity, we divide Set 1 into two subsamples, a high-metallicity sample (Set 1h) and a low-metallicity sample (Set 1l), using the midpoint of the metallicity distribution of Set 1, [Fe/H] = −0.12, as the dividing value.

3. DEBRIS DISK FREQUENCY AND DUST FLUX RATIO

The observed debris disk frequencies are listed in Tables 5–7. Due to the small sample size, the statistical uncertainties are calculated using a binomial distribution rather than the $\sqrt{N}$ Poisson uncertainty (see the appendix of Burgasser et al. 2003). Table 5 shows that the control sample (Set 1) has a debris disk frequency of $0.14^{-0.02}_{+0.03}$, similar to that found by the *Spitzer* surveys at 70 μm (Hillenbrand et al. 2008; Trilling et al. 2008; Carpenter et al. 2009). This result is also in agreement with Gaspar et al. (2013) who found a *Spitzer* incidence rate of 17.5% within the DUNES sample.

3.1. Dependence on Stellar Age

If debris disks evolve with time, and the samples compared have different age distributions within the decay timescale, this will introduce a bias in the comparison of the debris disk frequencies and dust flux ratios. As mentioned above, Figure 2 indicates that planet-bearing stars (Sets 3 and 4) tend to be older on average than the stars in the control samples because they are preferentially targeted by the Doppler studies.

To test for disk evolution, we divide the samples into stars with ages 0.1–1 Gyr (labeled as Sets 1y–5y) and stars older than 1 Gyr (Sets 1o–5o). We then compare the disk frequencies and dust flux ratios in the young and old samples, Sets 2y and 2o (lines 9 and 14 in Table 5). We do this exercise in the no-planet sample to minimize the effect of planet presence, as the goal is to check for disk evolution alone. Comparing Set 2y (with a disk frequency of 7/46 = 0.15) and Set 2o (with a disk frequency of 16/126 = 0.13) and using a binomial distribution, we find that detecting seven or more disks in Set 2y, when the expected detection rate is 0.13 (taking Set 2o as reference, i.e., the expected number of disk detections is 0.13·46), is a 39% probability event (24% if including the unconfirmed planetary systems—Table 8, lines 1 and 2). This probability is not low enough to claim that the higher incidence rate in the young sample compared to the old sample is significant .

The latter, however, does not take into account the uncertainty in the expected rate of the reference sample (in this case, Set 2o). The Fisher exact test is more appropriate in this regard. To carry out this test, we classify the stars in the

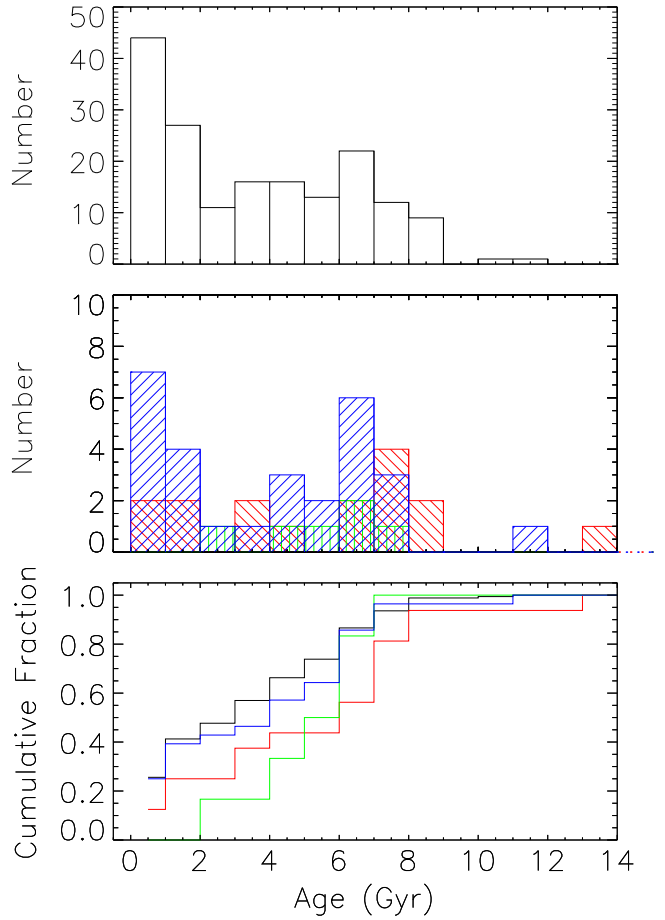

Figure 2. Distribution of stellar ages. Top: stars without known planets (Set 2). Middle: the line-filled colored histograms correspond to the high-mass planet sample (Set 3; in red, with hatching from the top left to the bottom right), low-mass planet sample (Set 4; in green, with vertical hatching) and debris disk sample (Set 5; in blue, with hatching from the top right to the bottom left). Bottom: cumulative distribution of stellar ages (same color code as above).

two samples in two categories regarding disk presence: stars with disks ($SNR_{dust} > 3$) and without disks ($SNR_{dust} < 3$). The null hypothesis in this case is that both sets (2y and 2o) are equally likely to harbor disks. The test gives a 60% probability to find the observed arrangement of the data if the null hypothesis were true (Table 8, lines 3 and 4). Note that the Fisher exact test can only reject the null hypothesis, never prove it true. The Fisher exact test in this case does not identify any evolution in disk frequency within the timescale considered.

A variable that is commonly used to characterize the strength of the disk emission is the dust flux ratio, $(F_{obs}^{100} - F_{star}^{100})/F_{star}^{100}$, where F_{obs}^{100} is the observed flux at 100 μm and F_{star}^{100} is the expected photospheric value at that wavelength. Table 3 lists the observed dust flux ratio for all the stars in our study. The 3σ upper limits (preceded by a "<" symbol) are given for stars without significant detected emission and are calculated assuming the observed flux is $F_{obs}^{100} + 3\sigma_{obs}^{100}$, for stars with $0 < F_{obs}^{100}/\sigma_{obs}^{100} < 3$, and $3\sigma_{obs}^{100}$, for stars with $F_{obs}^{100}/\sigma_{obs}^{100} < 0$.

Figure 3 shows the cumulative distribution of the dust flux ratio, whereas Figure 4 shows its dependency with stellar age. To assess quantitatively whether the data show a decay with time, we carry out survival analysis. This is favored over the K–S test because the latter does not deal with upper limits, and

Table 5
Debris Disk Frequency (at 100 μm)

	Set	Excluding Unconfirmed Planets[a]		Including Unconfirmed Planets[a]	
		No. of Excesses / No. of Stars	Excess Frequency[b] (at 100 μm)	No. of Excesses / No. of Stars	Excess Frequency[b] (at 100 μm)
1	1	29/204	$0.14^{-0.02}_{+0.03}$	29/204	$0.14^{-0.02}_{+0.03}$
2	2	24/182	$0.13^{-0.02}_{+0.03}$	22/179	$0.12^{-0.02}_{+0.03}$
3	3a,b	3/16	$0.19^{-0.06}_{+0.13}$	4/17	$0.23^{-0.07}_{+0.13}$
4	4	2/6	$0.33^{-0.13}_{+0.21}$	3/8	$0.37^{-0.13}_{+0.18}$
5	5	29/29	…	29/29	…
6	6	3/12	$0.25^{-0.08}_{+0.15}$	4/14	$0.29^{-0.09}_{+0.14}$
7	7	2/10	$0.20^{-0.07}_{+0.17}$	3/11	$0.27^{-0.09}_{+0.16}$
8	1y	7/48	$0.15^{-0.04}_{+0.07}$	7/48	$0.15^{-0.04}_{+0.07}$
9	2y	7/46	$0.15^{-0.04}_{+0.07}$	7/46	$0.15^{-0.04}_{+0.07}$
10	3aby	0/2	0	0/2	0
11	4y	0/0	…	0/0	…
12	5y	7/7	…	7/7	…
13	1o	21/146	$0.14^{-0.02}_{+0.03}$	21/146	$0.14^{-0.02}_{+0.03}$
14	2o	16/126	$0.13^{-0.02}_{+0.03}$	14/123	$0.11^{-0.02}_{+0.04}$
15	3abo	3/14	$0.21^{-0.07}_{+0.14}$	4/15	$0.27^{-0.08}_{+0.14}$
16	4o	2/6	$0.33^{-0.13}_{+0.21}$	3/8	$0.37^{-0.13}_{+0.18}$
17	5o	21/21	…	21/21	…
18	6o	3/10	$0.30^{-0.10}_{+0.17}$	4/12	$0.33^{-0.10}_{+0.15}$
19	7o	2/10	$0.20^{-0.07}_{+0.17}$	3/11	$0.27^{-0.09}_{+0.16}$

Notes.
[a] Unconfirmed planetary systems are HD 22049 (ϵ Eri), HD 10700 (τ Cet), and HD 189567.
[b] The statistical uncertainties are calculated using a binomial distribution.

a significant number of the targeted stars have $F_{100}/\sigma_{100} < 3$ (see Table 3 and down-facing arrows in Figure 4). Using ASURV 1.2 (Lavalley et al. 1992), which implements the survival analysis methods of Feigelson & Nelson (1985), we carried out the univariate, nonparametric two-sample Gehan, logrank, and Peto–Prentice tests to compute the probability that Sets 1y and 1o have been drawn from the same parent distribution with respect to the dust flux ratio. The results are listed in Table 8, line 5. The logrank test is more sensitive to differences at low values of the variable (i.e., near the upper limits), whereas the Gehan test is more sensitive to differences at the high end (i.e., at the detections; Feigelson & Nelson 1985). The Peto–Prentice test is preferred when the upper limits dominate and the sizes of the samples to be compared differ. The probabilities are not low enough to claim definitively that the two sets have been drawn from different distributions in terms of the dust flux ratio. However, given that they are in the 3–11% range to assess the role of planet presence, we will take the conservative approach of limiting the comparison of disk frequencies and dust flux ratios to stars with ages >1 Gyr (i.e., within Set 1o).

3.2. Dependence on Planet Presence

3.2.1. High-mass Planets

To assess the effect of high-mass planets on the presence of debris disks, we compare the disk frequencies in Set 3o (3/

Table 6
Dependence with Stellar Metallicity

Set	No. of Stars in Set	No. with High-mass Planets[a] ($>30\ M_\oplus$)	No. with Low-mass Planets[a] ($<30\ M_\oplus$)	No. with Debris Disks (at 100 μm)
1l ([Fe/H] $\leqslant -0.12$)	61	1	3 (5)	9
1h ([Fe/H] > -0.12)	75	14 (15)	3	17

Notes.
[a] Excluding unconfirmed planetary systems around HD 22049 (ϵ Eri), HD 10700 (τ Cet), and HD 189567. The parenthesis shows the result when including these three planetary systems.

Table 7
Debris Disk Frequency (at 100 μm) as a Function of Spectral Type

	Set	Total[a]		F-type[a]		G-type[a]		K-type[a]	
		No. of Excesses / No. of stars	Excess Frequency[b] (at 100 μm)	No. of Excesses / No. of stars	Excess Frequency[b] (at 100 μm)	No. of Excesses / No. of stars	Excess Frequency[b] (at 100 μm)	No. of Excesses / No. of stars	Excess Frequency[b] (at 100 μm)
1	1	29/204	$0.14^{-0.02}_{+0.03}$	10/46	$0.22^{-0.05}_{+0.07}$	11/61	$0.18^{-0.04}_{+0.06}$	8/97	$0.08^{-0.02}_{+0.04}$
2	2	24/182	$0.13^{-0.02}_{+0.03}$	9/42	$0.21^{-0.12}_{+0.08}$	7/48	$0.15^{-0.04}_{+0.06}$	8/92	$0.09^{-0.02}_{+0.04}$
3	3a,b	3/16	$0.19^{-0.06}_{+0.13}$	1/4	$0.25^{-0.10}_{+0.25}$	2/9	$0.22^{-0.08}_{+0.18}$	0/3	0
4	4	2/6	$0.33^{-0.13}_{+0.21}$	0/0	⋯	2/4	$0.5^{-0.2}_{+0.2}$	0/2	0
5	5	29/29	…	10/10	…	11/11	…	8/8	…
6	1o	21/146	$0.14^{-0.02}_{+0.03}$	8/33	$0.24^{-0.06}_{+0.09}$	7/49	$0.14^{-0.04}_{+0.06}$	6/64	$0.09^{-0.02}_{+0.05}$
7	2o	16/126	$0.13^{-0.02}_{+0.03}$	7/30	$0.23^{-0.06}_{+0.09}$	3/37	$0.08^{-0.03}_{+0.06}$	6/59	$0.10^{-0.04}_{+0.03}$
8	3abo	3/14	$0.21^{-0.07}_{+0.14}$	1/3	$0.33^{-0.14}_{+0.29}$	2/8	$0.25^{-0.09}_{+0.19}$	0/3	0
9	4o	2/6	$0.33^{-0.13}_{+0.21}$	0/0	⋯	2/4	$0.5^{-0.2}_{+0.2}$	0/2	0
10	5o	21/21	…	8/8	…	7/7	…	6/6	…

Notes.
[a] Excluding unconfirmed planetary systems around HD 22049 (ϵ Eri), HD 10700 (τ Cet), and HD 189567.
[b] The statistical uncertainties are calculated using a binomial distribution.

$14 = 0.21$) and Set 2o ($16/126 = 0.13$), limiting, for the reasons explained above, the comparison to the stars older than 1 Gyr. Using a binomial distribution, we find that detecting three or more disks in Set 3o when the expected detection rate is 0.13 (taking Set 2o as reference, i.e., the expected number of disk detections is 0.13·14) is a 27% event; the probability drops to 9% if including the unconfirmed planetary systems (Table 8, lines 9 and 10). Based on these numbers, there is no evidence that debris disks are more common around stars harboring high-mass planets compared to the average population, in agreement with previous studies based on *Spitzer* observations (Moro-Martín et al. 2007a; Bryden et al. 2009; Kóspál et al. 2009).

Classifying the stars in both samples (Sets 2o and 3o) into stars with and without disks and using the Fisher exact test, we find that there is a 41% probability to find the observed arrangement of the data if the null hypothesis were true, where the null hypothesis in this case is that the stars with at least one giant planet (Set 3o) and the stars without known-planet planets (Set 2o) are equally likely to harbor disks. This probability is 11% if including the unconfirmed planetary systems (Table 8, lines 11 and 12). The Fisher exact test, therefore, does not identify any correlation between debris disk frequency and high-mass planet presence. To test how different the disk frequencies would have to be for a correlation to be identified by the Fisher exact test, we carry out the test using Set 2o and a hypothetical Set 3o, varying in the latter the number of stars with and without disks: we find that the disk frequency for Set 3o would have to be about 2.8 times higher than in Set 2o. The identification of smaller differences in disk frequencies by the Fisher exact test is limited by low-number statistics.

Using survival analysis, we address whether the dust flux ratio, $F^{100}_{\rm dust}/F_{\rm star}$, is affected by the presence of high-mass planets. Figures 5 and 6 show the distribution of the dust flux ratio. The results from survival analysis (Table 8—lines 15 and 16) indicate that there is a high probability that the high-mass planet sample (Set 3o) and the no-planet sample (Set 2o) have been drawn from the same population in terms of the dust flux ratio at 100 μm (and the result holds if we include the unconfirmed planetary systems). The data do not show evidence that the disks around high-mass planet-bearing stars harbor more dust than those without known planets but with similar stellar characteristics.

3.2.2. Low-mass Planets

We now repeat the exercise above for the low-mass planet sample, comparing the disk frequency in Set 4o ($2/6 = 0.33$) to that in Set 2o ($16/126 = 0.13$). Using a binomial distribution, we find that detecting two or more disks in Set 4o when the expected number of disk detections is 0.13·6 (taking Set 2o as

Table 8
Results from the Statistical Tests

	Unconf. Planetary Systems[a]	Variable	Set A[b] $N_A^{\rm tot}(N_A^{\rm upl})$	Set B[b] $N_A^{\rm tot}(N_A^{\rm upl})$	Gehan[c]	Log-Rank[c]	Peto–Prentice[c]	K–S[d] Test	Fischer's[e] Exact Test	Poisson[f] Dist.	Binomial[g] Dist.
				Effect of Stellar Age on Disk Frequency and Flux Ratio							
1	N	Disk frequency	Set 2o	Set 2y	⋯	⋯	⋯	⋯	⋯	0.39	0.39
2	Y	Disk frequency	Set 2o	Set 2y	⋯	⋯	⋯	⋯	⋯	0.25	0.24
3	N	Disk presence[i]	Set 2o	Set 2y	⋯	⋯	⋯	⋯	0.62	⋯	⋯
4	Y	Disk presence[i]	Set 2o	Set 2y	⋯	⋯	⋯	⋯	0.60	⋯	⋯
5	⋯	$F_{\rm dust}/F_*$	Set 1o	Set 1y	0.10	0.03	0.11	⋯	⋯	⋯	⋯
	⋯	⋯	146(40)	48(18)	⋯	⋯	⋯	⋯	⋯	⋯	⋯
6	N	Disk frequency	Set 2oo	Set 2oy	⋯	⋯	⋯	⋯	⋯	0.37	0.36
7	N	Disk presence[i]	Set 2oo	Set 2oy	⋯	⋯	⋯	⋯	0.82	⋯	⋯
8	⋯	$F_{\rm dust}/F_*$	Set 1oo	Set 1oy	0.20	0.11	0.12	⋯	⋯	⋯	⋯
	⋯	⋯	71(18)	121(39)	⋯	⋯	⋯	⋯	⋯	⋯	⋯
				Effect of High-mass Planet Presence on Disk Frequency and Flux Ratio							
9	N	Disk frequency	Set 2o	Set 3o	⋯	⋯	⋯	⋯	⋯	0.25	0.27
10	Y	Disk frequency	Set 2o	Set 3o	⋯	⋯	⋯	⋯	⋯	0.07	0.09
11	N	Disk presence[i]	Set 2o	Set 3o	⋯	⋯	⋯	⋯	0.41	⋯	⋯
12	Y	Disk presence[i]	Set 2o	Set 3o	⋯	⋯	⋯	⋯	0.11	⋯	⋯
13	N	$F_{\rm dust}/F_*$	Set 2	Set 3	0.67	0.40	0.49	⋯	⋯	⋯	⋯
	⋯		182(62)	16(3)	⋯	⋯		⋯	⋯	⋯	⋯
14	Y	$F_{\rm dust}/F_*$	Set 2	Set 3	0.82	0.91	0.99	⋯	⋯	⋯	⋯
			179(62)	17(3)	⋯	⋯	⋯	⋯	⋯	⋯	⋯
15	N	$F_{\rm dust}/F_*$	Set 2o	Set 3o	0.56	0.59	0.48	⋯	⋯	⋯	⋯
	⋯	⋯	126(37)	14(3)	⋯	⋯	⋯	⋯	⋯	⋯	⋯
16	Y	$F_{\rm dust}/F_*$	Set 2o	Set 3o	0.92	0.82	0.87	⋯	⋯	⋯	⋯
	⋯	⋯	123(37)	15(3)	⋯	⋯	⋯	⋯	⋯	⋯	⋯
				Effect of Low-mass Planet Presence on Disk Frequency and Flux Ratio							
17	N	Disk frequency	Set 2o	Set 4o	⋯	⋯	⋯	⋯	⋯	0.18	0.18
18	Y	Disk frequency	Set 2o	Set 4o	⋯	⋯	⋯	⋯	⋯	0.06	0.05
19	N	Disk presence[i]	Set 2o	Set 4o	⋯	⋯	⋯	⋯	0.19	⋯	⋯
20	Y	Disk presence[i]	Set 2o	Set 4o	⋯	⋯	⋯	⋯	0.07	⋯	⋯
21	N	$F_{\rm dust}/F_*$	Set 2	Set 4	0.29	0.31	0.34	⋯	⋯	⋯	⋯
	⋯	⋯	182(62)	6(0)	⋯	⋯	⋯	⋯	⋯	⋯	⋯
22	Y	$F_{\rm dust}/F_*$	Set 2	Set 4	0.32	0.48	0.36	⋯	⋯	⋯	⋯
	⋯	⋯	179(62)	8(0)	⋯	⋯		⋯	⋯	⋯	
23	N	$F_{\rm dust}/F_*$	Set 2o	Set 4o	0.20	0.22	0.23	⋯	⋯	⋯	⋯
	⋯	⋯	126(37)	6(0)	⋯	⋯	⋯	⋯	⋯	⋯	⋯
24	Y	$F_{\rm dust}/F_*$	Set 2o	Set 4o	0.23	0.38	0.25	⋯	⋯	⋯	⋯
	⋯	⋯	123(37)	8(0)	⋯	⋯	⋯	⋯	⋯	⋯	⋯
				Effect of Planet Multiplicity on Disk Frequency and Flux Ratio							
25	N	Disk frequency	Set 6o	Set 7o	⋯	⋯	⋯	⋯	⋯	0.80	0.85
26	Y	Disk frequency	Set 6o	Set 7o	⋯	⋯	⋯	⋯	⋯	0.70	0.76

Table 8
(Continued)

	Unconf. Planetary Systems[a]	Variable	Set A[b] $N_A^{tot}(N_A^{upl})$	Set B[b] $N_A^{tot}(N_A^{upl})$	Gehan[c]	Log-Rank[c]	Peto–Prentice[c]	K–S[d] Test	Fischer's[e] Exact Test	Poisson[f] Dist.	Binomial[g] Dist.
27	N	Disk presence[i]	Set 6o	Set 7o	⋯	⋯	⋯	⋯	1.0	⋯	⋯
28	Y	Disk presence[i]	Set 6o	Set 7o	⋯	⋯	⋯	⋯	1.0	⋯	⋯
29	N	F_{dust}/F_*	Set 2o	Set 6o	0.78	0.57	0.62	⋯	⋯	⋯	⋯
	⋯		126(37)	10(2)	⋯	⋯	⋯	⋯	⋯	⋯	⋯
30	Y	F_{dust}/F_*	Set 2o	Set 6o	0.92	0.63	0.78	⋯	⋯	⋯	⋯
			123(37)	12(2)	⋯	⋯		⋯	⋯	⋯	⋯
31	N	F_{dust}/F_*	Set 2o	Set 7o	0.57	0.42	0.57	⋯	⋯	⋯	⋯
	⋯		126(37)	10(1)	⋯	⋯	⋯	⋯	⋯	⋯	⋯
32	Y	F_{dust}/F_*	Set 2o	Set 7o	0.30	0.27	0.31	⋯	⋯	⋯	⋯
	⋯		123(37)	11(1)	⋯	⋯		⋯	⋯	⋯	⋯
33	N	F_{dust}/F_*	Set 6o	Set 7o	0.66	0.22	0.56	⋯	⋯	⋯	⋯
	⋯		10(2)	10(1)	⋯	⋯	⋯	⋯	⋯	⋯	⋯
34	Y	F_{dust}/F_*	Set 6o	Set 7o	0.58	0.15	0.48	⋯	⋯	⋯	⋯
	⋯	⋯	12(2)	11(1)	⋯	⋯	⋯	⋯	⋯	⋯	⋯
				Effect of Planet Presence on Dust Temperature							
35	N	T_{dust}	Set 2t	Set 3t & Set 4t	⋯	⋯	⋯	0.80	⋯	⋯	⋯
	⋯	⋯	24	5	⋯	⋯	⋯	⋯	⋯		
36	Y	T_{dust}	Set 2t	Set 3t & Set 4t	⋯	⋯	⋯	0.93	⋯	⋯	⋯
	⋯	⋯	22	7	⋯	⋯	⋯	⋯	⋯	⋯	
				Effect of Stellar Metallicity on Disk Frequency and Flux Ratio							
37	⋯	Disk frequency	Set 1l	Set 1h	⋯	⋯	⋯	⋯	⋯	0.06	0.04
38	⋯	[Fe/H][h]	Set 1m-Set 5m	Set 5m	⋯	⋯	⋯	⋯	0.28	⋯	⋯
39	N	[Fe/H][h]	Set 1m-Set 3m	Set 3m	⋯	⋯	⋯	⋯	0.002	⋯	⋯
40	N	[Fe/H][h]	Set 1m-Set 4m	Set 4m	⋯	⋯	⋯	⋯	1.0	⋯	⋯
41	Y	[Fe/H][h]	Set 1m-Set 3m	Set 3m	⋯	⋯	⋯	⋯	0.0008	⋯	⋯
42	Y	[Fe/H][h]	Set 1m-Set 4m	Set 4m	⋯	⋯	⋯	⋯	0.47	⋯	⋯
43	N	[Fe/H]	Set 2 m	Set 3 m	⋯	⋯	⋯	0.002	⋯	⋯	
	⋯	⋯	115	15	⋯	⋯	⋯	⋯	⋯	⋯	⋯
44	N	[Fe/H]	Set 2 m	Set 4 m	⋯	⋯	⋯	0.49	⋯	⋯	⋯
	⋯	⋯	115	6	⋯	⋯	⋯	⋯	⋯	⋯	⋯
45	Y	[Fe/H]	Set 2 m	Set 3 m	⋯	⋯	⋯	0.005	⋯	⋯	⋯
	⋯	⋯	112	16	⋯	⋯	⋯	⋯	⋯	⋯	⋯
46	Y	[Fe/H]	Set 2 m	Set 4 m	⋯	⋯	⋯	0.32	⋯	⋯	⋯
	⋯	⋯	112	8	⋯	⋯	⋯	⋯	⋯	⋯	⋯
47	N	[Fe/H]	Set 2 m	Set 5 m	⋯	⋯	⋯	0.33	⋯	⋯	
	⋯	⋯	115	26	⋯	⋯	⋯	⋯	⋯	⋯	⋯
48	Y	[Fe/H]	Set 2 m	Set 5 m	⋯	⋯	⋯	0.39	⋯	⋯	⋯
	⋯	⋯	112	26	⋯	⋯	⋯	⋯	⋯	⋯	⋯
49	⋯	F_{dust}/F_*	Set 1h	Set 1h	0.42	0.27	0.44	⋯	⋯	⋯	⋯
	⋯	⋯	75(8)	61(5)	⋯	⋯	⋯	⋯	⋯	⋯	
				Effect of Spectral Type on Disk Frequency and Flux Ratio							
50	⋯	Disk frequency	Set 1o (G)	Set 1o (F)	⋯	⋯	⋯	⋯	⋯	0.10	0.08
51	⋯	Disk frequency	Set 1o (G)	Set 1o (K)	⋯	⋯	⋯	⋯	⋯	0.88	0.90
52	⋯	Disk frequency	Set 1o (K)	Set 1o (F)	⋯	⋯	⋯	⋯	⋯	0.01	0.008
53	⋯	Disk presence[i]	Set 1o (F+G)	Set 1o (K)	⋯	⋯	⋯	⋯	0.16	⋯	⋯
54	⋯	Disk presence[i]	Set 1o (F)	Set 1o (G+K)	⋯	⋯	⋯	⋯	0.09	⋯	⋯

Notes.

[a] Including unconfirmed planetary systems? "N" if those stars are included in the no-planet sample Set 2. "Y" if they are considered planet hosts (i.e., they are included in Sets 3 or 4 and 6 or 7).

[b] $N_A^{\rm tot}$ and $N_B^{\rm tot}$ are the total number of stars in each set (detections and nondetections). The number in parenthesis ($N_A^{\rm upl}$ and $N_B^{\rm upl}$) is the number of stars in each respective set with upper limits (i.e the number of stars with nondetections for which $F_{\rm obs}^{100}/\sigma_{\rm obs}^{100} < 3$).

[c] Results from the univariate, nonparametric two-sample Gehan, logrank, and Peto–Prentice tests, indicating the probability that Sets A and B have been drawn from the same population in terms of the variable under consideration.

[d] K–S test probability. This is the probability that the cumulative distributions of the variable under consideration in Sets A and B differ by more than the observed value D, where D is a measure of the largest difference between the two cumulative distributions. A small probability implies that the distributions could be significantly different.

[e] Fisher exact test two-tail probability.

[f] Using Poisson statistics, this is the cumulative probability of finding x or more disk detections (where x is the number of disk detections in Set B), when the expected rate is that of Set A.

[g] Using a binomial distribution, this is the probability of finding x or more disk detections (where x is the number of disk detections observed in Set B), when the expected rate is that of Set A.

[h] The Fisher exact test is calculated by dividing the samples into two groups: a high metallicity with [Fe/H] > –0.12 and a low metallicity with [Fe/H] ⩽ -0.12. The result is the probability that Sets A and B are equally likely to have the same distribution of high versus low [Fe/H].

[i] The Fisher exact test is calculated by dividing the samples into two groups: debris disk hosts, with a signal-to-noise ratio of the excess emission $\mathrm{SNR}_{\rm dust} = \frac{F_{\rm obs}^{100} - F_{\rm star}^{100}}{\sqrt{\sigma_{\rm obs}^{100^2} + \sigma_{\rm star}^{100^2}}} > 3$, and nondebris disk hosts, with $\mathrm{SNR}_{\rm dust} < 3$. The result is the probability that Sets A and B are equally likely to harbor debris disks.

Table 9
Debris Disk Properties (detected at 100 μm)

HIP	HD	GJ	UNS	$T_{\rm dust}^{\rm cold\,a}$ (K)	$R_{\rm dust}^{\rm cold\,a}$ (AU)
544	166	5	G030A	86.2 ± 2.0	8.3 ± 0.4
1368	···	14	K115A	29.0 ± 3.2	30.5 ± 6.8
4148	5133	42	K089A	29.2 ± 2.6	49.0 ± 8.7
5862	7570	55	F032A	73.8 ± 23.8	19.8 ± 12.8
7978	10647	3109	F051A	49.1 ± 3.6	40.3 ± 5.9
8102	10700	71	G002A	80.0 ±	8.5 ±
15510	20794	139	G005A	61.8 ± 14.1	16.5 ± 7.5
16537	22049	144	K001A	35.0 ±5.0	36.0 ±
16852	22484	147	F022A	98.0 ±7.7	14.4 ±2.3
17420	23356	···	K087A	59.3 ±83.3	12.0 ±33.8
17439	23484	152	···	41.0 ±	29.0 ±
22263	30495	177	G029A	70.6 ±2.7	15.3 ±1.2
23693	33262	189	F012A	115.0±11.7	7.2 ±1.5
26394	39091	9189	G085A	43.3 ±12.7	51.3 ±30.2
28103	40136	225	F028	149.0±	8.4 ±
32480	48682	245	F044A	51.9 ±3.1	39.3 ±4.8
42438	72905	311	G036A	87.2 ±9.5	10.2 ±2.2
43726	76151	327	G068A	87.0 ±19.6	10.4 ±4.7
61174	109085	471.2	F063A	37.4 ±1.9	124.6±13.4
62207	110897	484	F050A	53.7 ±8.3	28.2 ±8.8
64924	115617	506	G008A	66.8 ±3.1	15.9 ±1.5
65721	117176	512.1	···	100.0±	14.0 ±
71181	128165	556	K072A	42.5 ±59.7	21.0 ±59.1
71284	128167	557	F039A	126.8±34.1	9.1 ±4.9
85235	158633	675	K062A	62.0 ±16.2	13.0 ±6.8
107350	206860	836.7	G080A	86.6 ±8.7	11.0 ±2.2
107649	207129	838	G053A	44.1 ±1.6	45.2 ±3.4
114361	218511	1279	K114A	30.6 ±3.3	32.4 ±7.1
116771	222368	904	F021A	51.3 ±29.1	55.1 ±62.5

Notes.

[a] $T_{\rm dust}^{\rm cold}$ and $R_{\rm dust}^{\rm cold}$ for the stars with 100 μm excesses, calculated following Kennedy et al. (2012a, 2012b), using the full spectral energy distribution.

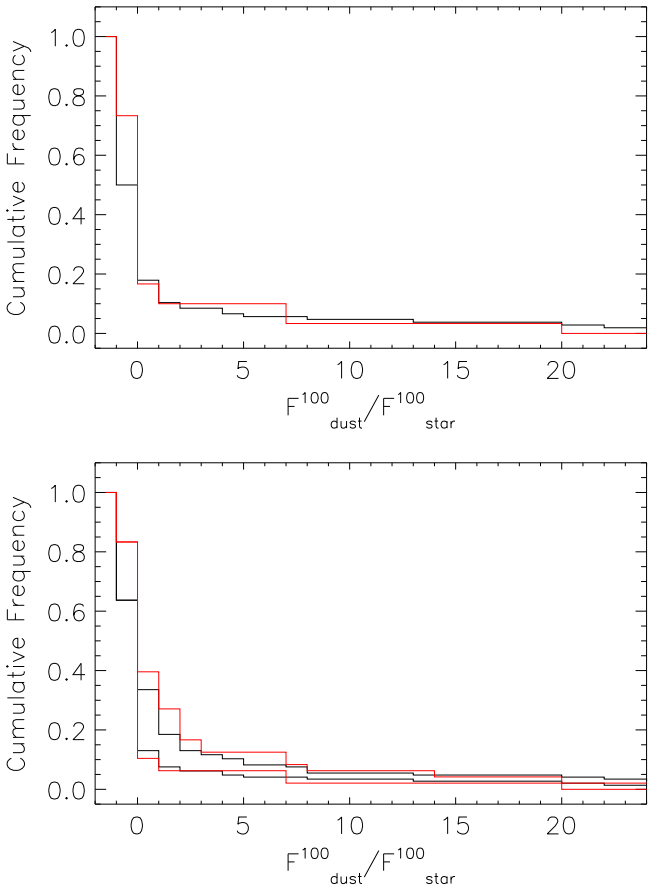

Figure 3. Cumulative frequency of the dust flux ratio at 100 μm. Top: only for the stars with significant detected emission (i.e., $F_{100}/\sigma_{100} > 3$—this panel is biased to large excesses because for stars with faint photospheres, they can be included only if they have large dust flux ratios). Bottom: for all the stars assuming an optimistic case, where the adopted flux ratio for the targets without significant detected emission is its corresponding upper limit, and a pessimistic case, where the adopted flux ratio is 0. Black is for the stars with ages >1 Gyr (Set 1o), and red is for stars with ages <1 Gyr (Set 1y).

reference) is a 18% probability event; the probability drops to 5% if including the unconfirmed planetary systems (Table 8, lines 17 and 18). Based on these numbers there is no firm evidence that debris disks are more common around stars harboring low-mass planets compared to the average population. This test, however, does not take into account the uncertainty in the expected rate of the reference sample.

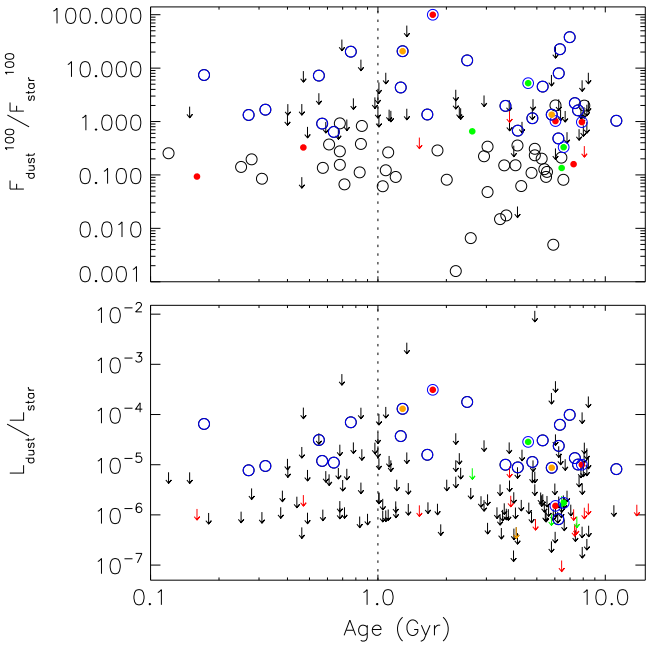

Figure 4. Top: dust flux ratio at 100 μm as a function of stellar age. The circles correspond to detections (i.e., $F_{100}/\sigma_{100} > 3$), whereas the down-facing arrows correspond to upper limits (i.e., $F_{100}/\sigma(F_{100}) < 3$). Black is for the stars without known planets (Set 2), red is for the high-mass planet sample (Set 3), and green is for the low-mass planet sample (Set 4). Unconfirmed planetary systems appear in orange. The larger open blue circles indicate which of those stars harbor excess emission at 100 μm (Set 5). Bottom: same as above but for the fractional luminosity, assuming a blackbody emission from the excess. The circles correspond to dust detections (i.e., stars with $\mathrm{SNR_{dust}} > 3$, where $\mathrm{SNR_{dust}} = \frac{F_{obs}^{100} - F_{star}^{100}}{\sqrt{\sigma_{obs}^{100\,2} + \sigma_{star}^{100\,2}}}$), whereas the down-facing arrows correspond to upper limits (i.e., $\mathrm{SNR_{dust}} < 3$).

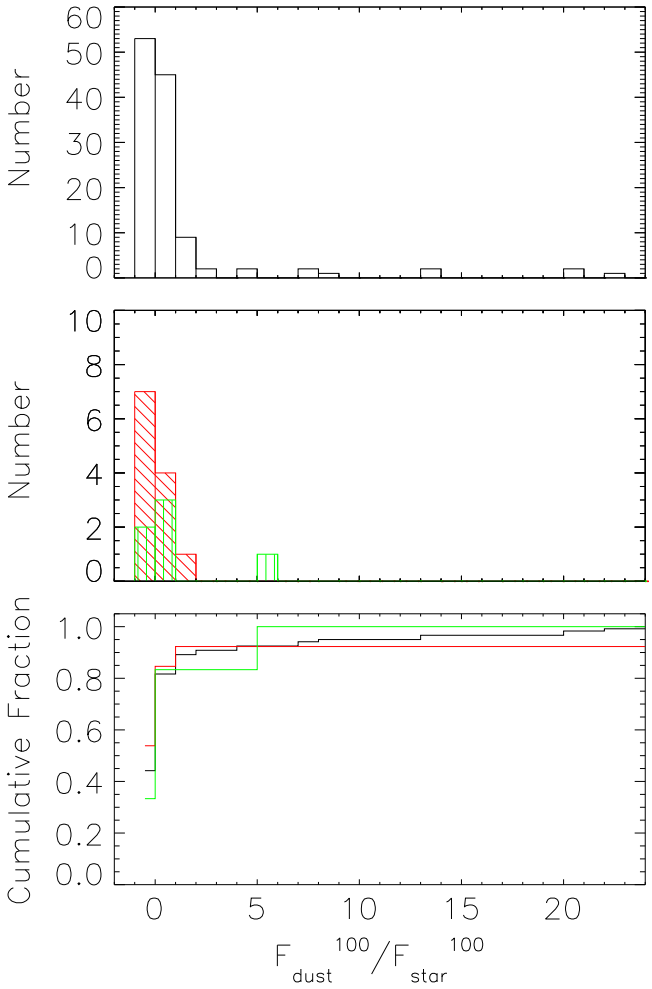

Figure 5. Distribution of the excess flux ratio at 100 μm for stars with significant detected emission (i.e., $F_{100}/\sigma_{100} > 3$). *Top*: the open black histogram corresponds to the stars without known planets (Set 2). *Middle*: the red filled histogram (with hatching from the top left to the bottom right) corresponds to the high-mass planet sample (Set 3), whereas the green filled histogram (with vertical hatching) corresponds to the low-mass planet sample (Set 4). *Bottom*: cumulative fraction (same color code as above). There are two stars outside the plotted range, one in Set 3 a with $F_{dust}^{100}/F_{star}^{100} = 99.8$ and another in Set 2 with $F_{dust}^{100}/F_{star}^{100} = 38.0$.

The Fisher exact test gives in a 19% probability to find the observed arrangement of the data if the null hypothesis were true, where the null hypothesis is that the stars with low-mass planets only (Set 4o) and the stars without planets (Set 2o) are equally likely to harbor disks. The probability drops to 7% when including the unconfirmed planetary systems (Table 8, lines 19 and 17). We find that the disk frequency for Set 4o would have to be about four times higher than in Set 2o in order for the Fisher exact test to identify a correlation in our small subsample, Set 4o. The identification of smaller differences in disk frequencies is limited by low-number statistics.

The results from survival analysis (Table 8—lines 23 and 24) indicate that the probability that the low-mass planet sample (Set 4o) and the no-planet sample (Set 2o) have been drawn from the same population in terms of the dust flux ratio at 100 μm is not low enough to claim a correlation (even when including the unconfirmed planetary systems). However, in this case, survival analysis might be unreliable because of the small sample size ($N \lesssim 10$) of the low-mass planet sample.

In Section 5.2 below we discuss that there are hints that the debris disk frequency around F-type stars might be higher than around G- and K-type, although this trend is not found to be statistically significant. However, given that none of the F-type stars in our sample harbor planets (see Figure 11, because it is not possible to search to such low masses around them), to be conservative we now compare the low-mass planet sample to a control sample that does not include F-type stars. We find that the binomial-derived probability that the disk frequencies of the low-mass planet sample and the no-planet sample (excluding the F's) are similar is 9% (compared to 14% when including the F's). The Fisher exact probability gives 12% (compared to 19% when including the F's). Therefore, our conclusion that there is no evidence of correlation does not change when excluding F-type stars.

In summary, our study does not show evidence of a correlation, but our conclusion is limited by the small sample size.

3.2.3. Planetary System Multiplicity

Comparing Set 6o (single-planet sample, with a disk frequency of 0.3) and Set 7o (multiple-planet sample, with a disk frequency of 2/10 = 0.20) and using a binomial distribution, we find that detecting two or more disks in Set 7o, when the expected detection rate is 0.30 (taking Set 6o as reference, i.e., the expected number of disk detections is 0.30·10), is an 85% probability event (changing only slightly

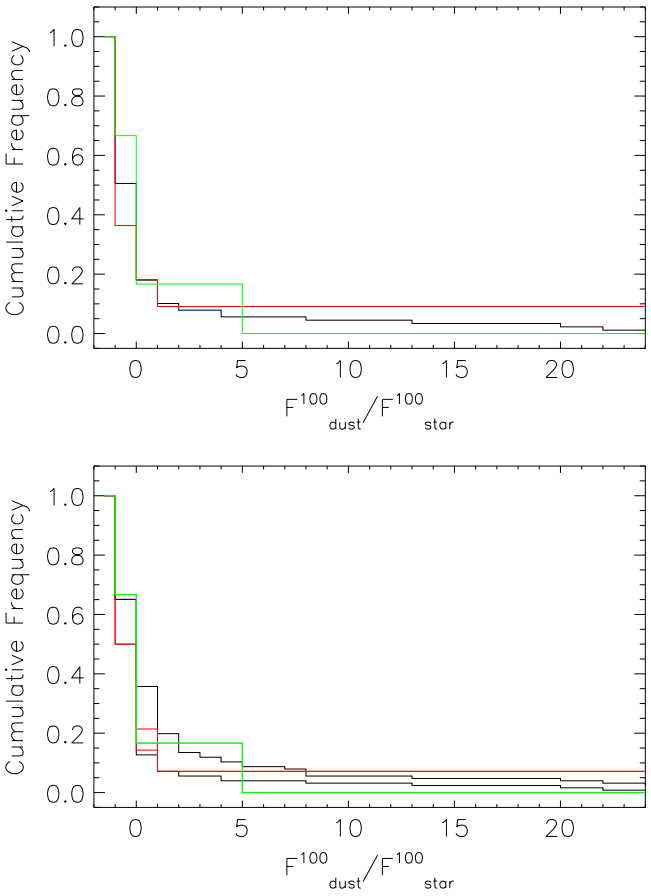

Figure 6. Cumulative frequency of the dust flux ratio at 100 μm. Top: only for the stars with significant detected emission (i.e., $F_{100}/\sigma_{100} > 3$). Bottom: for all the stars assuming an optimistic case, where the adopted flux ratio for the targets without significant detected emission is its corresponding upper limit, and a pessimistic case, where the adopted flux ratio is 0. Black is for the stars without known planets with ages >1 Gyr (Set 2o), red is for stars harboring high-mass planets (Set 3o), and green is for those harboring low-mass planets (Set 4o). The unconfirmed planetary systems are included under Set 2 (no-planet sample).

when including the unconfirmed planetary systems—Table 8, lines 25 and 26). The data do not show any evidence that debris disks are more or less common around stars harboring multiple-planet systems compared to single-planet systems. The same conclusion results from the Fisher exact test (Table 8, lines 27 and 28). Regarding the dust flux ratio, survival analysis results (Table 8, lines 29–34) indicate that the multiple-planet, single-planet, and no-planet samples could have been drawn from the same population in terms of the dust flux ratio at 100 μm (and the result holds if we include the unconfirmed planetary systems). The data, again, do not show evidence of any correlation between planet multiplicity and the strength of the debris disk emission.

3.2.4. Effect on the Characteristic Dust Temperature

We now assess whether there is any evidence that the debris disks around planet-bearing stars might be different from those around an average population of stars in terms of the characteristic dust temperature. Sets labeled with a "t" include only the stars with estimated dust temperatures (listed in Table 9). The calculation of the graybody dust temperatures is described in Kennedy et al. (2012a) based on observations with a wide wavelength coverage. Figure 7 shows the distribution of the characteristic dust temperature in the no-planet sample (Set 2t) and the planet samples (Sets 3 t and 4t). The K–S test yields two values, D, a measure of the largest difference between the two cumulative distributions under consideration, and the probability of finding a D-value greater than the observed value; the latter is an estimate of the significance level of the observed value of D as a disproof of the null hypothesis that the distributions come from the same parent population, that is, a small probability implies that the distributions could be significantly different. The result from the K–S test is shown in Table 8 (lines 35 and 36), showing a very high probability. The calculation of the probability is good if $N_1N_2/(N_1 + N_2) \geqslant 4$, where N_1 and N_2 are the number of stars in each set. However, if one wants to be conservative, it might be compromised when $N < 20$, as it is the case here. Based on the limited information we have so far, there is no evidence that the characteristic temperature of the debris disks around planet-bearing stars differs from the rest.

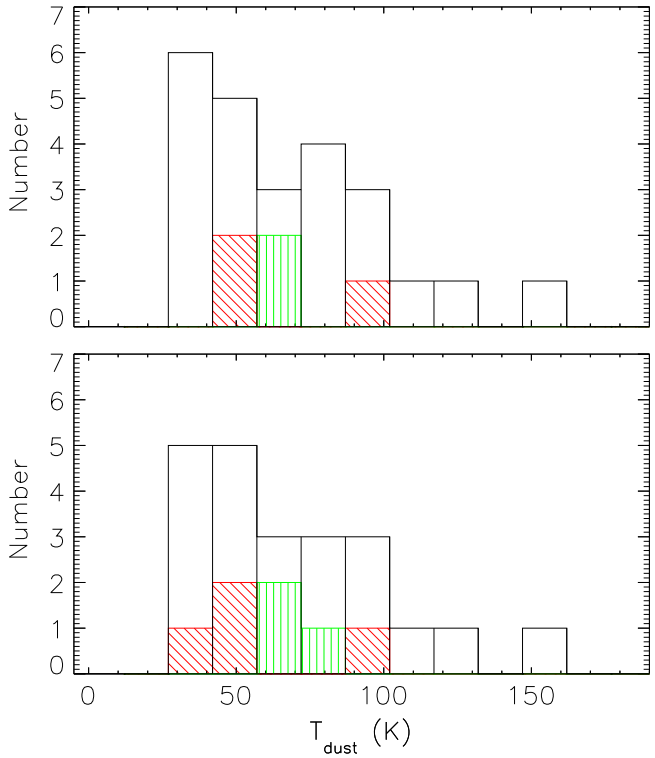

Figure 7. Distribution of the estimated blackbody dust temperature for the stars with debris disk detections at 100 μm (i.e., $SNR_{dust} > 3$). The open black histogram corresponds to stars without known planets (Set 2t), whereas the line-filled colored histogram corresponds to stars harboring high-mass planets (Set 3t; in red, with hatching from the top left to the bottom right) and stars harboring low-mass planets (Set 4t; in green, with vertical hatching). The top panel excludes unconfirmed planetary systems ϵ Eri and τ Cet, whereas the bottom panel includes both planetary systems.

4. CORRELATIONS WITH STELLAR METALLICITY

Figure 8 shows the distribution of stellar metallicity. To assess the correlation with metallicity, we create Sets 1m–5 m, constituted by stars in Sets 1–5 with known metallicities[25] from

[25] Regarding possible sources of biases due to stellar age and distance, Maldonado et al. (2012) argued that because the stars are at close distances from the Sun (in our case within 20 pc), it is unlikely that they have suffered different enrichment histories.

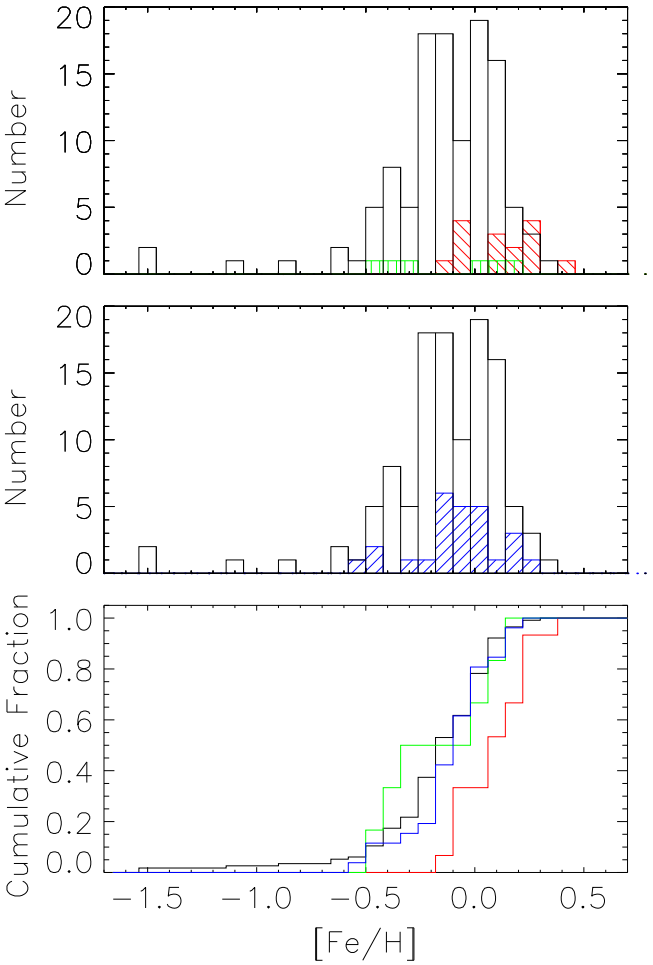

Figure 8. Distribution of stellar metallicities (logarithmic scale, with [Fe/H] = 0.0 for solar metallicity). The open black histograms correspond to stars without known planets and with known metallicities (Set 2m). Top: the line-filled colored histograms correspond to stars harboring high-mass planets (Set 3m; in red, with hatching from the top left to the bottom right) and low-mass planets (Set 4m; in green, with vertical hatching). Middle: subset harboring excess emission at 100 μm (Set 5m; in blue, with hatching from the bottom left to the top right). The stars with unconfirmed planetary systems, ϵ Eri and τ Cet, are included in Set 2m (no-planet sample). Bottom: cumulative distributions of stellar metallicities (same color code as above).

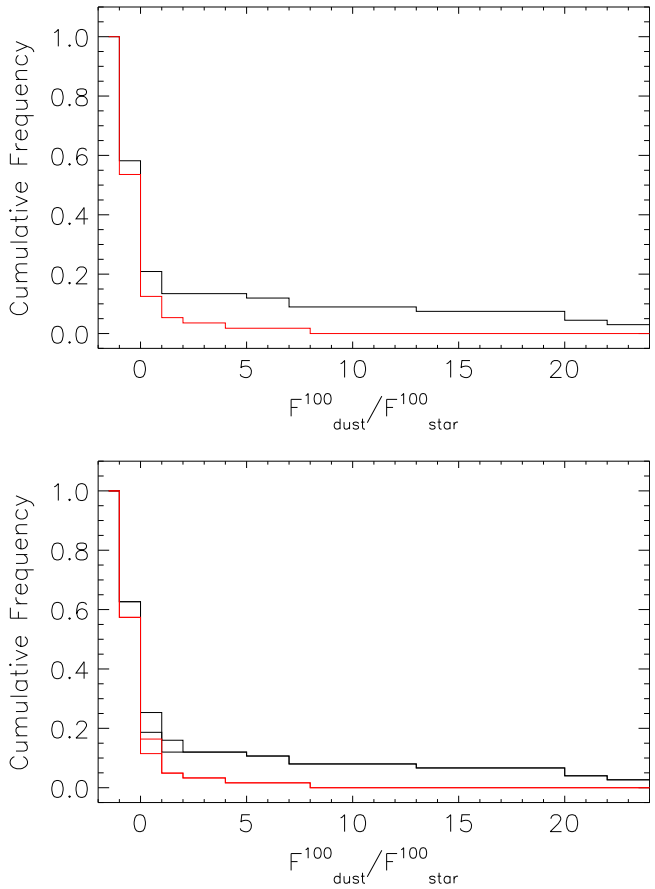

Figure 9. Cumulative frequency of the dust flux ratio at 100 μm. Top: only for the stars with significant detected emission (i.e., $F_{100}/\sigma_{100} > 3$). Bottom: for all the stars assuming an optimistic case, where the adopted flux ratio for the targets without significant detected emission is its corresponding upper limit, and a pessimistic case, where the adopted flux ratio is 0. Black is for the stars with metallicities larger than the average ([Fe/H] > −0.12; Set 1h), and red is for the stars with lower metallicities ([Fe/H] ⩽ −0.12; Set 1l), independently of planet presence.

Maldonado et al. (2012) and Eiroa et al. (2013). These sets are further divided into stars with high metallicities (Sets 1h–5h) and those with low metallicities (Sets 1l–5l), using the midpoint of the metallicity distribution, [Fe/H] = −0.12, as the dividing value. Table 6 lists how many stars are in each subset.

4.1. Debris Disk Presence

We now compare the debris disk frequencies in Set 1h (17/75 = 0.23) and Set 1l (9/61 = 0.15). Using a binomial distribution, finding 17 or more disk detections in Set 1h, when the expected detection rate is 0.15 (taking Set 1l as reference, i.e., the expected number of disk detections is 0.15·75), is a 4% probability event (Table 8—line 37), indicating that the disk frequencies in the high- and low-metallicity samples might differ. This result, however, does not take into account the uncertainty in the expected rate of the reference sample (in this case Set 1l). From the Fisher exact test, we find that there is a 28% probability to find the observed arrangement of the data if the null hypothesis were true, where the null hypothesis in this case is that the stars without disks (Set 1m–Set 5m) and the stars with disks (Set 5m) are equality likely to have metallicities > −0.12 (Table 8—line 38). From the K–S test, the probability that the no-planet sample (Set 2m) and the debris disk sample (Set 5m) could have been drawn from the same distribution in terms of stellar metallicity is 33% (39% when including unconfirmed planetary systems; Table 8—lines 47–48).

Regarding the strength of the excess emission, we use survival analysis to check if the low-metallicity and high-metallicity samples could have been drawn from the same population in terms of the dust flux ratio. Figures 9 and 10 show the cumulative frequencies of the dust flux ratio and the fractional luminosity of Sets 1h and 1l, showing that there is a dearth of debris disks with high dust flux ratios and high fractional luminosities around low-metallicity stars. However, the probabilities listed in Table 8 (line 49) indicate that this trend is not statistically significant. We cannot rule out the hypothesis that the high-metallicity and low-metallicity samples have been drawn from the same distribution in terms of the dust flux ratio. We conclude that the Fisher exact test and survival analysis do not allow us to identify any correlation between high stellar metallicity and debris disks.

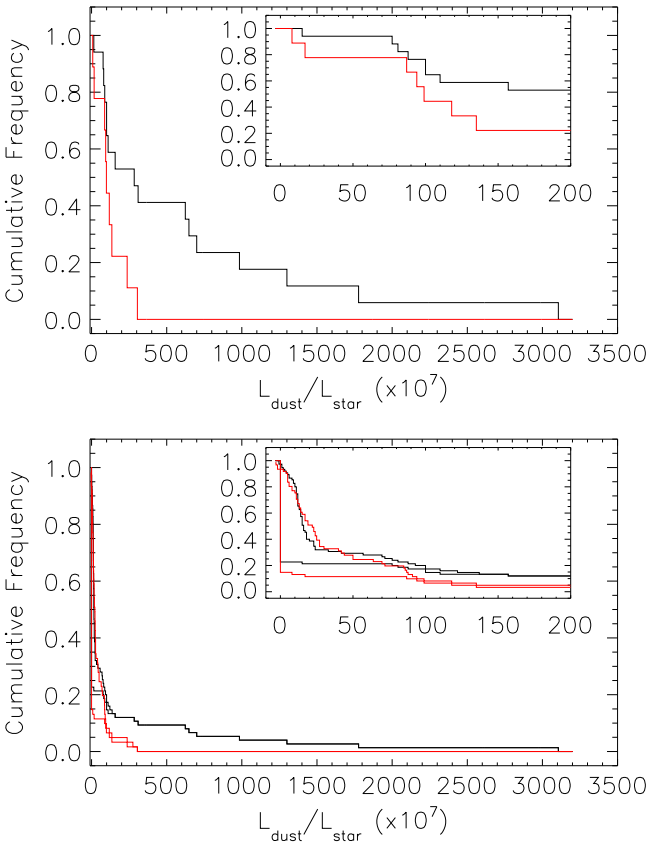

Figure 10. Cumulative frequency of the dust fractional luminosity. Top: only for the stars with excess detections (i.e., stars with $SNR_{dust} > 3$). Bottom: for all the stars assuming an optimistic case, where the adopted fractional luminosity for the targets without excess detections is its corresponding upper limit, and a pessimistic case, where the adopted fractional luminosity is 0. Black is for the stars with metallicities larger than the average ([Fe/H] > −0.12; Set 1h), and red is for the stars with lower metallicities ([Fe/H] ⩽ −0.12; Set 1l), independently of planet presence.

4.2. Planet Presence

Comparing the planet and no-planet samples in terms of stellar metallicity with the Fisher exact test (Table 8—lines 39–42), we find that in the case of giant planets, there is a 0.2% probability to find the observed arrangement if the stars without giant planets (Set 1m-Set 3m) and the stars with giant planets (Set 3m) were equally likely to have metallicities > -0.12, whereas for low-mass planets (Set 1m-Set 4 versus Set 4), this probability is almost 100% (the result holds when including the unconfirmed planetary systems). From the K–S test, the probability that the no-planet sample and the high-mass planet sample could have been drawn from the same distribution in terms of stellar metallicity is 0.2%, whereas the probability that the no-planet sample has been drawn from the same distribution as the low-mass planet sample and the debris disk sample is much larger (49%; Table 8—lines 43–46).

5. POSSIBLE BIASES INTRODUCED BY THE SAMPLE SELECTION

5.1. Presence of Undetected Planets

We now describe the potential biases that the sample selection could introduce in the statistical analysis described above. First, we assess whether the presence of unidentified planetary systems could affect our results. If we were to have many stars with high-mass planets in the control sample, Set 2, one could argue that a high-mass planet–debris disk correlation could have been present but hidden by all the "planet contaminants." However, because the high-mass planet frequency is small, this seems unlikely. Due to the higher frequency of low-mass planets (Mayor et al. 2009, 2011; Batalha 2014 and references therein; Marcy et al. 2014 and references therein), we probably have many stars with low-mass planets in the control sample which have not been identified. This means that a low-mass planet–debris disk correlation may still be hidden in the data. We could avoid these biases by comparing the planet sets to a subset of stars in Set 2 for which the presence of planets within a given period and mass has been ruled out by the radial velocity surveys. However, because nondetections are generally not made public by the planet search teams, the information to construct this no-planet stellar sample is not available.

5.2. Distribution of Spectral Types

By considering FGK stars to assess the planet–debris disk correlation, we are implicitly assuming that the disk frequency and the planet frequency do not differ significantly among these spectral types.

Table 7 and Figure 11 show the distribution of spectral types in the samples under consideration. Let us limit the comparison to stars older than 1 Gyr (to avoid biases due to disk evolution), i.e., to the stars in Set 1o (Table 7—line 6). For the F-stars, the disk fraction is 0.24 (8/33 disk detections): using a binomial distribution, finding eight or more disk detections, when the expected detection rate is 0.14 (taking the disk frequency of the G-stars as reference, i.e., when the expected number of disk detections is 0.14·33), is an 8% probability event. Whereas for the K-stars, with a disk fraction of 0.09 (6/64 disk detections), using a binomial distribution, finding six or more disk detections, when the expected detection rate is 0.14, is a 90% probability event. If we were to take the disk frequency of K-type as reference, for the F-stars, finding eight or more disk detections, when the expected detection rate is 0.09 (expected number of disk detections of 0.09·33), would be a 0.8% event (Table 8—lines 50–52). The latter seems to indicate there is a significant difference in disk frequencies between K-type and F-type stars.

Eiroa et al. (2013) found that the frequency of disks in the DUNES survey does not change significantly among FGK stars. The increased disk frequency for F-type stars found in our sample might have been biased to some degree by the shallower integration time of some of the DEBRIS targets, although the different $T_{\rm eff}$ distribution for the stars in the DEBRIS and DUNES surveys may also play a role (the former covering all FGK stars, whereas the latter covers mid-F to mid-K.[26] Using a larger sample of *Spitzer* and *Herschel* observations, Sierchio et al. (2014) found no significant dependence with spectral type in the F4–K4 range.

The test above does not consider the uncertainty in the expected rate of the reference sample. Classifying the stars into those with and without debris disks and applying the Fisher exact test, we find that in this case the probability is not low enough to disprove the null hypothesis that the F-stars are

[26] The spectral type dependence of the debris disk frequency within the DEBRIS sample will be studied in more detail by B. Sibthorpe et al. (2015, in preparation).

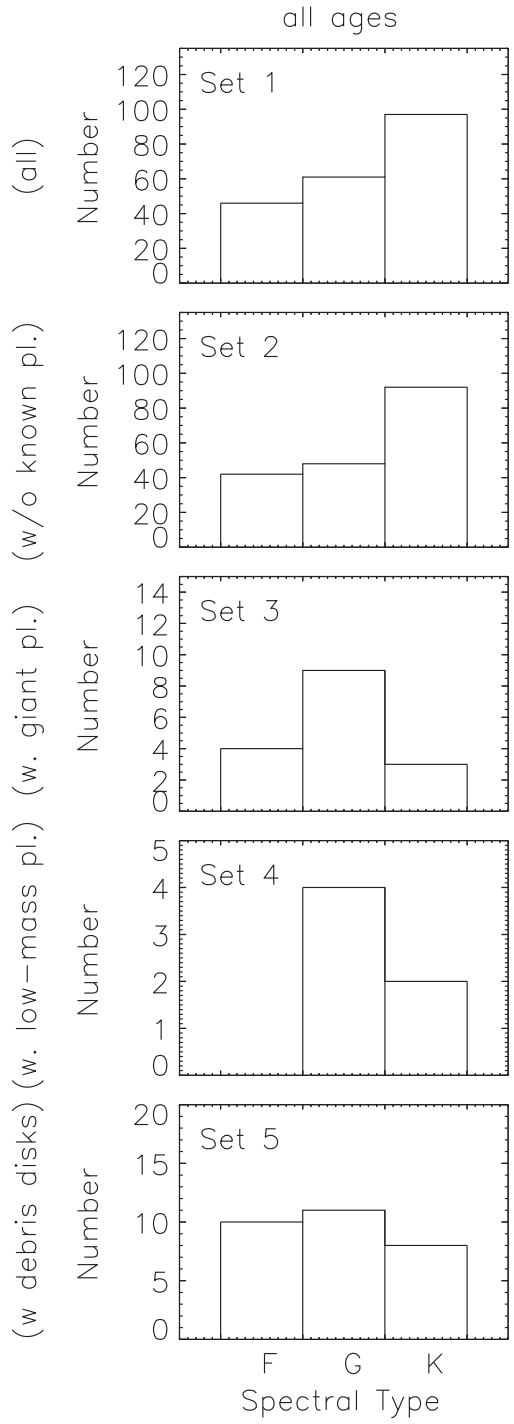

Figure 11. Distribution of spectral types for the different sets.

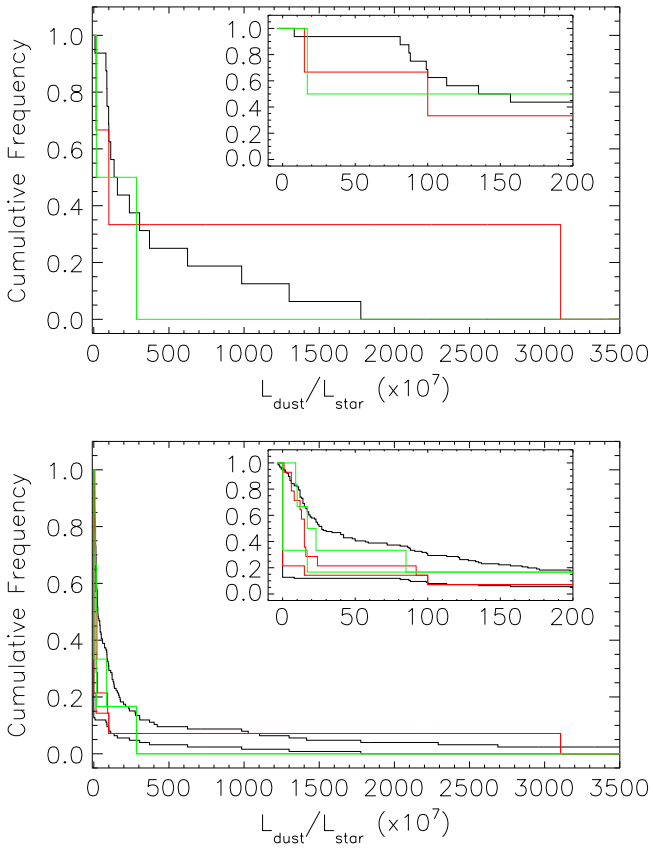

Figure 12. Cumulative frequency of the dust fractional luminosity. Top: only for the stars with excess detections (i.e., stars with $SNR_{dust} > 3$). Bottom: for all the stars assuming an optimistic case, where the adopted fractional luminosity for the targets without excess detections is its corresponding upper limit, and a pessimistic case, where the adopted fractional luminosity is 0. Black is for the stars without known planets with ages >1 Gyr (Set 2o), red is for stars harboring high-mass planets (Set 3o), and green is for those harboring low-mass planets (Set 4o). The unconfirmed planetary systems are included under Set 2 (no-planet sample).

equally likely to harbor disks as are the G+K stars (Table 8—lines 53 and 54).

Regarding planet frequency, Doppler surveys indicate there is a correlation between high-mass planet frequency and spectral type that follows roughly a linear increase with stellar mass (Johnson et al. 2010). From a compilation of Doppler surveys, Gaidos et al. (2013) suggest $f(\%) = -1.11 + 5.33\, M_{star}/M_{\odot}$, for planets > 8 $R_{\oplus}$ (masses >95 $M_{\oplus}$—see their Figure 8). For low-mass planets in the 0.8–6 $R_{\oplus}$ range, *Kepler* data indicate that among the FGK stars the planet frequency does not depend significantly on the spectral type (Fressin et al. 2013). Table 7 and Figure 11 indicate that neither the high-mass nor low-mass planet frequencies within our sample reflect the above trends, with a higher incidence around G-type stars mostly likely because fewer F and Ks were searched for planets. This might skew slightly the disk incidence rate comparison for high-mass planets. Again, because nondetections are generally not made public, there is no way to circumvent this issue.

In Section 7.6 we discuss how the conclusions change when excluding F-type stars from our analysis.

6. FRACTIONAL LUMINOSITIES AND COMPARISON TO THE SOLAR SYSTEM'S DEBRIS DISK

Figure 12 shows the cumulative frequency of the dust fractional luminosity. This variable is commonly used to characterize debris disk emission because it allows comparison of disks observed at different wavelengths; it is not very model-dependent as long as the wavelength coverage is good (as is the case in our samples). For stars with dust excess detections ($SNR_{dust} > 3$), the fractional luminosity is calculated following Kennedy et al. (2012a, 2012b). For stars with dust excess nondetections ($SNR_{dust} < 3$), the 3σ upper limit to the fractional luminosity is calculated from

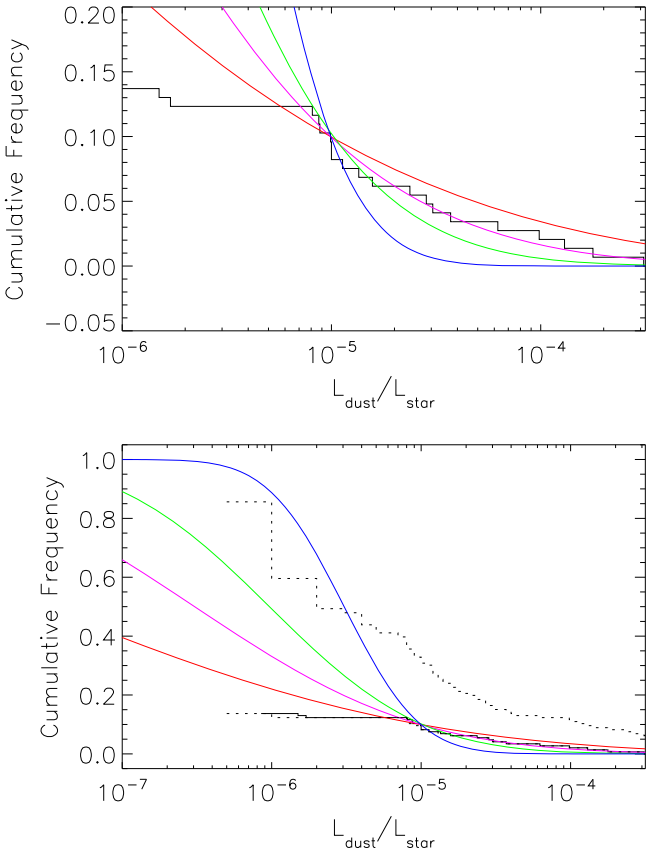

Figure 13. Cumulative frequency of the fractional luminosity. The thick black histogram corresponds to the stars with ages >1 Gyr independently of planet presence (Set 1o). Because we are interested in the cumulative frequency of the stars for fractional luminosities greater than the minimum observed value, in calculating the cumulative distribution we adopt the pessimistic case, where the fractional luminosity for the stars without excess is 0. The blue, green, magenta, and red lines correspond to theoretical distributions that assume a Gaussian distribution of fractional luminosities in logarithmic scale, with average values of 10×, 3×, 1×, and 0.1× that of the solar system, respectively, and assuming for the solar system a fractional luminosity of $10^{-6.5}$. We fixed the cumulative frequency of disks with $L_{dust}/L_{*} > 10^{-5}$ at 10% according to the observed result (in set 1o), implying 1σ widths for the theoretical distributions of 0.4, 0.8, 1.18, and 2.0 for the blue, green, magenta, and red lines, respectively. Top: showing only the detected range; there are only three targets with fractional luminosities below 8×10^{-6}, compromising the fit to the data in that low range because of low-number statistics. Bottom: the dotted line that coincides with the solid line corresponds to the the pessimistic case, where the adopted fractional luminosities for the targets without excess detections are taken to be 0, whereas the second dotted line on the upper part of the panel corresponds to the optimistic case, for which the upper limits are adopted.

$\frac{L_{dust}}{L_{star}} = \left(\frac{T_{dust}}{T_{star}}\right)^4 \left(\frac{e^{x_{dust}}-1}{e^{x_{star}}-1}\right) F_{obs}^{100} - F_{star}^{100} \cdot F_{star}^{100}$ following Equation (4) in Beichman et al. (2006), and assuming the observed flux is $F_{obs}^{100} + 3\sigma_{obs}^{100}$, for stars with $F_{obs}^{100}/\sigma_{obs}^{100} > 0$, and $3\sigma_{obs}^{100}$, for stars with $F_{obs}^{100}/\sigma_{obs}^{100} < 0$. In this expression, $x = \frac{h\nu}{kT}$, where ν is the frequency corresponding to 100 μm, $T_{star} = T_{eff}$ is the effective stellar photospheric temperature, and T_{dust} is assumed to be 50 K (as in Eiroa et al. 2013).

The fractional luminosity can help place the debris disk observations in this study in the context of the solar system's debris disk. Following Bryden et al. (2006), we compare the observed cumulative distribution of fractional luminosity to those expected from Gaussian distributions in logarithmic scale, with average values of 10×, 3×, 1×, and 0.1× that of the solar system's debris disk, assuming for the latter a fractional luminosity of $10^{-6.5}$. To avoid biases due to disk evolution, we limit the comparison to stars older than 1 Gyr (Set 1o). The observed and Gaussian-derived cumulative distributions are shown in Figure 13. The bottom panel shows that the blue line exceeds the most optimistic case at low fractional luminosities. This means that we can reject the hypothesis that the median of the disk fractional luminosity is 10 times that of the solar system's debris disk, in agreement with Bryden et al. (2006). The best fit to the data is a Gaussian centered on the solar system value (magenta line in the top panel). This result is discussed in Section 7.7.

7. SUMMARY AND DISCUSSION

We have carried out a statistical study of an unbiased subsample of the *Herschel* DEBRIS and DUNES surveys, consisting of 204 FGK stars located at distances <20 pc, with ages >100 Myr and with no binary companions at <100 AU. The main goal is to assess whether the frequency and properties of debris disks around a control sample of FGK stars are statistically different from those around stars with high-mass and low-mass planets. We find the following results.

7.1. Disk Evolution

The *Spitzer* surveys found that the upper envelope of the 70 μm debris disk emission shows a decline over the ~100 Myr of a star's lifetime, indicating that there might be a population of rapidly evolving disks that disperse by 100 Myr. Our sample does not show clear evidence of disk evolution on the gigayear timescale. This is in agreement with the lack of disk evolution observed at 70 μm in *Spitzer* surveys for stars older than 1 Gyr[27] (Hillenbrand et al. 2008; Trilling et al. 2008; Carpenter et al. 2009). In a recent study, using both *Spitzer* and *Herschel* observations, and using a sample 2.5 times larger than ours, Sierchio et al. (2014) found that for disks with fractional luminosities smaller than 10^{-5} there is a significant decrease in the debris disk frequency between 3 and 5 Gyr. To look for evidence of disk evolution in the 5 Gyr timescale that could bias our results, we have divided the sample into stars with ages 0.1–5 Gyr (labeled as Sets 1oy and 2oy) and stars older than 5 Gyr (Sets 1oo and 2oo). We then compare the disk frequencies and dust flux ratios in both subsamples (lines 6 and 8 in Table 8). The overall resulting probabilities are not low enough to claim that the two sets have been drawn from different distributions in terms of the dust flux ratio, nor that their disk incidence rates differ significantly. The Fisher exact test (line 7 in Table 8) also indicates that both sets are equally likely to harbor disks. We therefore do not find evidence in our restricted sample of disk evolution in the 5 Gyr timescale.

7.2. High-mass Planet Presence

Our sample does not show evidence that debris disks are more common around stars harboring high-mass planets compared to the average population. This is in agreement with the studies based on *Spitzer* observations that found no correlation between fractional luminosities, L_{dust}/L_{star}, and the presence of high-mass planets (Moro-Martín et al. 2007a; Bryden et al. 2009). Figure 8 in Maldonado et al. (2012) also

[27] Compared to the 70 μm observations, the 100 μm emission might also trace dust located further out, where the collision times are longer; if this second population of dust exists, one would expect even less evolution at this longer wavelength.

shows this trend, where the stars with disks and planets seem to be well mixed with stars with only disks in terms of the fractional luminosity, but they did not carry out any statistical analysis. This issue will be revisited using a larger sample that combines *Herschel* DEBRIS, DUNES, and SKARPS observations (G. Bryden et al. 2015, in preparation).

Overall, the lack of observed correlation between high-mass planets and debris disks was understood within the context of the core accretion model for planet formation, where the conditions to form debris disks are more easily met than the conditions to form high-mass planets. This is in agreement with the metallicity studies that indicate that there is a correlation between high-mass planets and stellar metallicity, but no correlation between debris disks and stellar metallicity. Additionally, the presence of debris disks around stars with a very wide range of properties, from M-type (Kennedy et al. 2007; Lestrade et al. 2012) to the progenitors of white dwarfs (Jura 2003, 2007), implies that planetesimal formation is a robust process that can take place under a wide range of conditions. Therefore, based on formation conditions, if planetesimals can be common in systems with and without high-mass planets, there is no reason to expect a correlation between high-mass planets and debris disks (Moro-Martín et al. 2007a).

Another factor contributing to the lack of a well-defined correlation with planet presence might be that the dynamical histories likely vary from system to system, and other stochastic effects need also to be taken into account, e.g., those produced by dynamical instabilities of multiple-planet systems clearing the outer planetesimal belt (Raymond et al. 2011, 2012), the planetesimal belt itself triggering planet migration and instabilities (Tsiganis et al. 2005; Levison et al. 2011), or the stripping of planetesimals from disks during stellar flybys in the first 100 Myr, when systems are still in their dense birth cluster (Lestrade et al. 2011).

Another aspect that needs to be taken into account is that the planets detected by radial velocity surveys and the dust observed at 100 μm occupy well-separated regions of space, limiting the influence of the observed closer-in planets on the dust production rate of the outer planetesimal belt; there are long-range gravitational perturbations produced by secular perturbations from single planets on eccentric orbits (Mustill & Wyatt 2009) or multiplanet systems (Moro-Martín et al. 2007b, 2010) that allow close-in planets to excite outer planetesimal belts, but the timescale of the former may be longer than the age of the system, and the latter is limited to certain planet configurations.

7.3. Low-mass Planet Presence

In a preliminary study, and using a different subsample of the *Herschel* DEBRIS survey, Wyatt et al. (2012) identified a tentative correlation between debris and the presence of planets with masses $<95\,M_{\oplus}$. Using a different subsample, Marshall et al. (2014) also found evidence that stars with planets $<30\,M_{\oplus}$ are more likely to harbor debris disks than are stars with planets $>30\,M_{\oplus}$ (6/11 versus 5/26). There are aspects related to the dynamical evolution of planetary systems that could result in a higher frequency of debris disks around stars with low-mass planets compared to those with high-mass planets. Wyatt et al. (2012) discussed two alternative scenarios: (1) if the planets formed in the outer region and migrated inward, low-mass planets would have been inefficient at accreting or ejecting planetesimals, leaving them on dynamically stable orbits over longer timescales; high-mass planets would have been more efficient at ejecting planetesimals, leaving behind a depleted population of dust-producing parent bodies. (2) Alternatively, if the planets formed in situ, the timescale for the planet to eject the planetesimals is shorter in systems with high-mass planets than with low-mass planets. However, the true migration histories of the systems studied may be significantly more complicated than the story portrayed under the two scenarios described above. For example, in our own solar system, it is now well established that the ice giants, Uranus and Neptune, migrated outward over a significant distance to reach their current locations, sculpting the trans-Neptunian population as they did so (Hahn & Malhotra 2005).

In this paper we have used the cleanest possible sample of the *Herschel* DEBRIS and DUNES surveys to assess if the data at hand can confirm the tentative detection of a low-mass planet–debris correlation. Contrary to the preliminary analyses mentioned above, here we have discarded stars without known ages, with ages <1 Gyr, and with binary companions <100 AU, allowing us to rule out possible correlations due to effects other than planet presence. We find that the data do not show clear evidence that debris disks are more common around stars harboring low-mass planets compared to the average population. However, having a clean sample comes at a price because the smaller sample size limits the strength of the statistical result: a positive detection of a correlation could have been detected by the Fisher exact test only if the disk frequency around low-mass planet stars were to be about four times higher than the control sample.

The planet–debris disk correlation studies can shed light on the formation and evolution of planetary systems and may perhaps help "predict" the presence of planets around stars with certain disk characteristics. Far from being a closed issue, this correlation (or lack of) needs to be revisited. In the near future, G. Bryden et al. (2015, in preparation) will address this question using a sample that combines *Herschel* DEBRIS, DUNES and *SKARPS* surveys, overcoming to some degree our limitations due to the small sample size. However, there are another two aspects that need to be improved upon and, with the data at hand, cannot be addressed at the moment: our ability to detect fainter disks and to detect or rule out the presence of lower-mass planets to greater distances.

Regarding the disk detections, our knowledge of circumstellar debris is limited: we only have detections for the top 20% of the dust distribution, assuming all stars have a remnant circumstellar disk at some level; limits closer to the KB-level are only possible for nearby F+ type stars, and we are incapable of seeing exact analogues to our own solar system leaving a large parameter space with no constraint on planet or dust properties. Future missions under consideration such as *SPICA* would improve things significantly: if its telescope is not descoped, the improvement in sensitivity would allow detection of photospheres not detected by *Herschel*, e.g., for M stars and for FGK stars at large distances; its noise would also be lower than *Herschel*, allowing it to detect fainter disks.

Regarding the planet detection, the high frequency of low-mass planets indicates that we probably have many low-mass planet stars in the control sample which have not been identified, hindering our ability to detect a correlation. To overcome this problem, we rely on radial velocity surveys to

gradually probe both to greater distances and lower planet masses; but also critically important is that these teams make the nondetections publicly available so we can identify systems for which the presence of planets of a given mass can be excluded out to a certain distance.

7.4. Planetary System Multiplicity

Dynamical simulations by Raymond et al. (2011, 2012) of multiple-planet systems with outer planetesimal belts indicate that there might be a correlation between the presence of multiple planets and debris. This is because the presence of the former indicates a dynamically stable environment where dust-producing planetesimals may have survived for extended periods of time (as opposed to single-planet systems that in the past may have experienced gravitational scattering events that resulted in the ejection of other planets and dust-producing planetesimals). It is of interest therefore to assess whether debris disks are correlated with planet multiplicity.

Our sample does not show evidence that debris disks are more or less common, or more or less dusty, around stars harboring multiple-planet systems compared to single-planet systems.

7.5. Dust Temperature

Based on the limited statistics, there is no evidence that the characteristic dust temperature of the debris disks around planet-bearing stars is any different from that in debris disks without identified planets. This is of course subject to detailed individual modeling, as the spatial dust disk distribution of the planet-bearing systems might show more structural features due to gravitational perturbations compared to the disks around stars not harboring planets, in which case it might not be appropriate to describe the dust excess emission with a single temperature.

7.6. Stellar Metallicity

We find that there is no evidence that debris disks are more common around stars with high metallicities. This is in agreement with previous studies (Bryden et al. 2006; Greaves et al. 2006). We find a dearth of debris disks with high dust flux ratios (also fractional luminosities) around low-metallicity stars, consistent with the model of Wyatt et al. (2007). However, survival analysis tests indicate that this trend is not statistically significant and that we cannot rule out the hypothesis that the high-metallicity and low-metallicity samples have been drawn from the same distribution in terms of the dust flux ratio.

The data confirm the well-known correlation between high metallicities and the presence of high-mass planets. On the contrary, we find no evidence of a correlation between high metallicities and the presence of low-mass planets. We therefore find the well-known positive correlation between the presence of planets and stellar metallicity for stars with high-mass planets but no correlation for stars with low-mass planets only in agreement with extensive Doppler studies (Santos et al. 2004; Fisher & Valenti 2005; Ghezzi et al. 2010; Mayor et al. 2011). Maldonado et al. (2012) studied a larger stellar sample and derived the metallicities in a uniform way. They found an increasing correlation with stellar metallicity from stars without planets and disks and stars with debris disks to stars with high-mass planets. They also concluded that the correlation with stellar metallicity is due to the presence of planets and not the presence of debris disks.

7.7. Fractional Luminosity and Comparison to the Solar System Debris Disk

Comparing the observed cumulative distribution of fractional luminosity to those expected from a Gaussian distribution in logarithmic scale, we find that a distribution centered on the solar system value (taken as $10^{-6.5}$) fits the data well, whereas one centered at 10 times the solar system's debris disks can be rejected.

This is of interest in the context of future prospects for terrestrial planet detection. Even though the *Herschel* observations presented in this study trace cold dust located at tens of AU from the star, for systems with dust at the solar system level, the dust dynamics is dominated by Poynting–Robertson drag. This force makes the dust in the outer system drift into the terrestrial-planet region. This warm dust can impede the future detection of terrestrial planets due to the contaminant exozodiacal emission, with its median level, its uncertainty, and shape of its distribution being some of the parameters that may affect the aperture size required for a telescope such as *ATLAST* to be able to characterize biosignatures (see, e.g., Stark et al. 2014; Brown 2015). Ruling out a distribution of fractional luminosities centered at 10 times the solar system level implies that there are a large number of debris disk systems with dust levels in the KB region low enough not to become a significant source of contaminant exozodiacal emission. Comets and asteroids located closer to the star are other sources of dust that can contribute to the exozodiacal emission (and for those, *Herschel* observations do not provide constraints), but planetary systems with low KB dust-type of emission likely imply low-populated outer belts leading to low cometary activity. These results, therefore, indicate that there are good prospects for finding a large number of debris disk systems (i.e., systems with evidence of harboring planetesimals) with exozodiacal emission low enough to be appropriate targets for terrestrial planet searches. Dedicated warm dust surveys with the Keck Interferometer Nuller (Millan-Gabet et al. 2011), CHARA/FLUOR (Absil et al. 2013), VLTI/PIONIER (Ertel et al. 2014), and LBTI (under the HOSTS program) are shedding or will soon shed light on this issue.

Even though the planetesimals detected by Herschel in the far infrared are located far from the terrestrial-planet region, their presence is favorable to the growth and survival of terrestrial planets because these planetesimals indicate that the system has experienced a calm dynamical evolution, as opposed to an environment of dynamically active, high-mass planets. Such an environment would tend to destroy both the outer, dust-producing planetesimal belt and the planetesimals that might otherwise build the terrestrial planets. This conclusion was the result of Raymond et al.'s (2011, 2012) extensive dynamical simulations consisting of high-mass planet embryos and inner and outer belts of planetesimals. These simulations find that there is a strong correlation between the presence of cold dust in the outer planetary system and the presence of terrestrial planets in the inner region, so a system with low levels of KB dust emission might also imply a dynamical history not amicable to terrestrial planets. The solar system, in this case, would be an outlier, with a low-level of KB dust but a high number of terrestrial planets. It would be of great interest to extend Raymond et al.'s (2011, 2012)

simulations to cover a wider range of initial conditions to further explore this correlation, as it would enlighten the target selection for an *ATLAST*-type mission.

A.M.-M. thanks Ewan Cameron for insightful comments and the STScI Directors Discretionary Research fund for support. J. P.M. is a UNSW Vice Chancellor's Postdoctoral Research Fellow. G.K. and M.C.W.'s work was supported by the European Union through ERC Grant 279973. C.E. and B.M. are partially supported by Spanish Ministry of Economy Grant AYA 2011-26202. D.R.R. acknowledges support from Chilean FONDECYT Grant 3130520. M.B. acknowledges support from a FONDECYT Postdoctoral Fellowship, Project 3140479.

REFERENCES

Absil, O., Defrère, D., Coudé du Foresto, V., et al. 2013, A&A, 555, A104
Batalha, N. M. 2014, PNAS, 111, 12647
Beichman, C. A., Bryden, G., Rieke, G. H., et al. 2005, ApJ, 622, 1160
Beichman, C. A., Bryden, G., Stapelfeldt, K. R., et al. 2006, ApJ, 652, 1674
Booth, M., Wyatt, M. C., Morbidelli, A., Moro-Martín, A., & Levison, H. F. 2009, MNRAS, 399, 385
Brogi, M., Snellen, I. A. G., de Kok, R. J., et al. 2012, Natur, 486, 502
Brown, R. A. 2015, ApJ, 799, 87
Bryden, G., Beichman, C. A., Trilling, D. E., et al. 2006, ApJ, 636, 1098
Bryden, G., Beichman, C. A., Carpenter, J. M., et al. 2009, ApJ, 705, 1226
Buchhave, L. A., Latham, D. W., Johansen, A., et al. 2012, Natur, 486, 375
Burgasser, A. J., Kirkpatrick, J. D., Reid, I. N., et al. 2003, ApJ, 586, 512
Butler, R. P., Wright, J. T., Marcy, G. W., et al. 2006, ApJ, 646, 505
Carpenter, J. M., Bouwman, J., Mamajek, E. E., et al. 2009, ApJS, 181, 197
Duchêne, G. 2010, ApJL, 709, L114
Eggenberger, A., Udry, S., Chauvin, G., et al. 2007, A&A, 474, 273
Eggenberger, A., Udry, S., Chauvin, G., et al. 2011, in IAU Symp. 276, The Astrophysics of Planetary Systems: Formation, Structure, and Dynamical Evolution, ed. A. Sozzetti, M. G. Lattanzi, & A. P. Boss (Cambridge: Cambridge Univ. Press), 409
Eiroa, C., Fedele, D., Maldonado, J., et al. 2010, A&A, 518, L131
Eiroa, C., Marshall, J. P., Mora, A., et al. 2013, A&A, 555, A11
Endl, M., Robertson, P., Cochran, W. D., et al. 2012, ApJ, 759, 19
Ertel, S., Absil, O., Defrère, D., et al. 2014, A&A, 570, A128
Feigelson, E. D., & Nelson, P. I. 1985, ApJ, 293, 192
Fischer, D. A., & Valenti, J. 2005, ApJ, 622, 1102
Fressin, F., Torres, G., Charbonneau, D., et al. 2013, ApJ, 766, 81
Gaidos, E., Fischer, D. A., Mann, A. W., & Howard, A. W. 2013, ApJ, 771, 18
Gáspár, A., Rieke, G. H., & Balog, Z. 2013, ApJ, 768, 25
Ghezzi, L., Cunha, K., Smith, V. V., et al. 2010, ApJ, 720, 1290
Greaves, J. S., Fischer, D. A., & Wyatt, M. C. 2006, MNRAS, 366, 283
Gregory, P. C., & Fischer, D. A. 2010, MNRAS, 403, 731
Hahn, J. M., & Malhotra, R. 2005, AJ, 130, 2392
Hatzes, A. P., Cochran, W. D., McArthur, B., et al. 2000, ApJL, 544, L145
Hillenbrand, L. A., Carpenter, J. M., Kim, J. S., et al. 2008, ApJ, 677, 630
Jewitt, D., Moro-Martìn, A., & Lacerda, P. 2009, in The Kuiper Belt and Other Debris Disks, ed. H. A. Thronson, M. Stiavelli, & A. Tielens (Dordrecht: Springer Netherlands), 53
Johnson, J. A., Aller, K. M., Howard, A. W., & Crepp, J. R. 2010, PASP, 122, 905
Johnson, J. A., Payne, M., Howard, A. W., et al. 2011, AJ, 141, 16
Jura, M. 2003, ApJL, 584, L91
Jura, M., Farihi, J., & Zuckerman, B. 2007, ApJ, 663, 1285
Kennedy, G. M., Kenyon, S. J., & Bromley, B. C. 2007, Ap&SS, 311, 9
Kennedy, G. M., Wyatt, M. C., Sibthorpe, B., et al. 2012a, MNRAS, 426, 2115
Kennedy, G. M., Wyatt, M. C., Sibthorpe, B., et al. 2012b, MNRAS, 421, 2264
Kóspál, Á., Ardila, D. R., Moór, A., & Ábrahám, P. 2009, ApJL, 700, L73
Krivov, A. V. 2010, RAA, 10, 383
Lavalley, M., Isobe, T., & Feigelson, E. 1992, in ASP Conf. Ser. 25, Astronomical Data Analysis Software and Systems I, ed. D. M. Worrall, C. Biemesderfer, & J. Barnes (San Francisco, CA: ASP), 245
Lestrade, J.-F., Morey, E., Lassus, A., & Phou, N. 2011, A&A, 532, A120
Lestrade, J.-F., Matthews, B. C., Sibthorpe, B., et al. 2012, A&A, 548, A86
Levison, H. F., Morbidelli, A., Tsiganis, K., Nesvorný, D., & Gomes, R. 2011, AJ, 142, 152
Lisse, C. M., Beichman, C. A., Bryden, G., & Wyatt, M. C. 2007, ApJ, 658, 584
Lovis, C., Mayor, M., Pepe, F., et al. 2006, Natur, 441, 305
Maldonado, J., Eiroa, C., Villaver, E., Montesinos, B., & Mora, A. 2012, A&A, 541, A40
Marcy, G. W., Weiss, L. M., Petigura, E. A., et al. 2014, PNAS, 111, 12655
Marshall, J. P., Moro-Martín, A., Eiroa, C., et al. 2014, A&A, 565, A15
Matthews, B. C., Krivov, A. V., Wyatt, M. C., Bryden, G., & Eiroa, C. 2014, arXiv:1401.0743
Matthews, B. C., Sibthorpe, B., Kennedy, G., et al. 2010, A&A, 518, L135
Mayor, M., Udry, S., Lovis, C., et al. 2009, A&A, 493, 639
Mayor, M., Marmier, M., Lovis, C., et al. 2011, arXiv:1109.2497
Millan-Gabet, R., Serabyn, E., Mennesson, B., et al. 2011, ApJ, 734, 67
Moro-Martin, A. 2013, in Planets, Stars, and Planetary Systems, ed. T. D. Oswalt, L. M. French, & P. Kalas (Dordrecht: Springer Netherlands), 431
Moro-Martín, A., & Malhotra, R. 2003, AJ, 125, 2255
Moro-Martín, A., Malhotra, R., Bryden, G., et al. 2010, ApJ, 717, 1123
Moro-Martín, A., Carpenter, J. M., Meyer, M. R., et al. 2007a, ApJ, 658, 1312
Moro-Martín, A., Malhotra, R., Carpenter, J. M., et al. 2007b, ApJ, 668, 1165
Mustill, A. J., & Wyatt, M. C. 2009, MNRAS, 399, 1403
Pepe, F., Correia, A. C. M., Mayor, M., et al. 2007, A&A, 462, 769
Pepe, F., Lovis, C., Ségransan, D., et al. 2011, A&A, 534, A58
Phillips, N. M., Greaves, J. S., Dent, W. R. F., et al. 2010, MNRAS, 403, 1089
Raymond, S. N., Armitage, P. J., Moro-Martín, A., et al. 2011, A&A, 530, A62
Raymond, S. N., Armitage, P. J., Moro-Martín, A., et al. 2012, A&A, 541, A11
Rodriguez, D. R., & Zuckerman, B. 2012, ApJ, 745, 147
Santos, N. C., Israelian, G., Randich, S., García López, R. J., & Rebolo, R. 2004, A&A, 425, 1013
Sierchio, J. M., Rieke, G. H., Su, K. Y. L., & Gáspár, A. 2014, ApJ, 785, 33
Stark, C. C., Roberge, A., Mandell, A., & Robinson, T. D. 2014, ApJ, 795, 122
Tinney, C. G., Wittenmyer, R. A., Butler, R. P., et al. 2011, ApJ, 732, 31
Trilling, D. E., Bryden, G., Beichman, C. A., et al. 2008, ApJ, 674, 1086
Tsiganis, K., Gomes, R., Morbidelli, A., & Levison, H. F. 2005, Natur, 435, 459
Tuomi, M., Jones, H. R. A., Jenkins, J. S., et al. 2013, A&A, 551, A79
Vican, L. 2012, AJ, 143, 135
Vitense, C., Krivov, A. V., Kobayashi, H., & Löhne, T. 2012, A&A, 540, A30
Vogt, S. S., Wittenmyer, R. A., Butler, R. P., et al. 2010, ApJ, 708, 1366
Wang, J., Xie, J.-W., Barclay, T., & Fischer, D. A. 2014, ApJ, 783, 4
Wittenmyer, R. A., Endl, M., & Cochran, W. D. 2007, ApJ, 654, 625
Wittenmyer, R. A., Endl, M., Cochran, W. D., Levison, H. F., & Henry, G. W. 2009, ApJS, 182, 97
Wright, J. T., Marcy, G. W., Butler, R. P., et al. 2008, ApJL, 683, L63
Wright, J. T., Upadhyay, S., Marcy, G. W., et al. 2009, ApJ, 693, 1084
Wyatt, M. C. 2008, ARA&A, 46, 339
Wyatt, M. C., Clarke, C. J., & Greaves, J. S. 2007, MNRAS, 380, 1737
Wyatt, M. C., Kennedy, G., Sibthorpe, B., et al. 2012, MNRAS, 424, 1206